Supergene minerals with Indium (In) in the San Roque polymetallic project, North Patagonian Massif, Argentina

Verónica BOUHIER[1,2*], M. Florencia GARGIULO[1,2], Corina PADELLETTI DI MARCO[1], Gabriela FERRACUTTI[1,2]

1 Departamento de Geología, Universidad Nacional del Sur, San Juan 670, Bahía Blanca, Argentina.

2 Instituto Geológico del Sur (INGEOSUR, CCT CONICET Bahía Blanca - UNS), Av. Alem 1253 cuerpo B' 1er. piso, Bahía Blanca, Argentina.

*E-mail: vbouhier@gmail.com

Número total de páginas: 28

Número total de figuras: 8

Número total de cuadros: 0

Encabezado sugerido: Supergene minerals in the San Roque project, North Patagonian Massif.

ABSTRACT

San Roque (40°45’54"S; 65º48'07"W) is a mining project located in the eastern sector of Northpatagonian Massif, Río Negro province, Patagonia, Argentina. In this project the polymetallic mineralization has epithermal characteristics and is hosted in the jurassic volcanites, volcanoclastites and sedimentary rocks of the Marifil Volcanic Complex. It was defined as a low to intermediate sulfidation epithermal system in which the ore mineral association mainly consists of native gold, low Fe In-bearing sphalerite, chalcopyrite and galena. This contribution documents the geochemical data and the mineralogical studies carried out in representative samples of two drillholes that intercepted Del Indio Structure in the supergene oxidation zone. This structure represents one of the most explored epithermal manifestations of the project. According to the observations with a scanning electron microscope and semi-quantitative analyses, the main supergene minerals that concentrate In, Cu, Zn, Pb, Ga, Mn, P, As and Cl are attributed to hematite, plumbojarosite, coronadite and mottramite, which are hosted by coarse-grained epiclastic subfacies from the Marifil Volcanic Complex, described in this contribution as polymictic orthobreccia. It is also documented, for the first time, a supergene mineral-association together with base and precious metals, by oxidation of the polymetallic epithermal mineralization in the San Roque project. The veinlets, stockwork and, in a lesser extent, disseminated mineralization style of the hypogene ore, with In-bearing sphalerite and pyrite as the predominant sulfides, combined with the porosity and limited acid-buffering capacity of the host rock, favored the penetration of acidic, and oxidizing relatively V-rich meteoric waters, giving rise the and subsequent oxidation process.

Keywords: Critical metals, supergene ore, vanadate, Jurassic, Patagonia.

RESUMEN

Minerales supergénicos con Indio (In) en el proyecto polimetálico San Roque, Macizo Nordpatagónico, Argentina. San Roque (40º45’54"S; 65º48'07"W) es un proyecto minero

ubicado en el sector oriental del Macizo Norpatagónico, provincia de Río Negro, Patagonia, Argentina. En este proyecto la mineralización tiene características epitermales y polimetálicas y está alojada en las volcanitas, volcanoclastitas y sedimentitas del Jurásico correspondientes al Complejo Volcánico Marifil. Fue definido como un sistema epitermal de baja a intermedia sulfuración en el cual la asociación mineral de mena consiste principalmente en oro nativo, esfalerita con In y pobre en Fe, calcopirita y galena. En esta contribución se documentan datos geoquímicos y estudios mineralógicos realizados en muestras representativas de dos sondajes que interceptaron la Estructura Del Indio en la zona de oxidación supergénica. Esta estructura representa una de las manifestaciones epitermales más exploradas del proyecto. De acuerdo a las observaciones con microscopio electrónico de barrido y análisis-semicuantitativos, los principales minerales supergénicos que concentran In, Cu, Zn, Pb, Ga, Mn, P, As y Cl se atribuyen a hematita, mottramita, plumbojarosita y coronadita, que se alojan principalmente en facies epiclásticas de grano grueso del Complejo Volcánico Marifil, descriptas en esta contribución como orthobrechas polimícticas. Asimismo se presenta, por primera vez, una asociación mineral supergénica portadora de In, metales base y preciosos, generada a partir de la oxidación de la mineralización epitermal polimetálica en el proyecto San Roque. El estilo vetiforme, en *stockwork* y en menor medida, diseminado de la mineralización primaria con esfalerita, con esfalerita con In y pirita, como los sulfuros predominantes, combinados con la porosidad y la capacidad limitada de la roca de caja de actuar como *buffer*, favorecieron la penetración de fluidos meteóricos ácidos, oxidantes, relativamente ricos en V, que dieron lugar al posterior proceso de oxidación.

Palabras clave: Metales estratégicos, mena supergénica, vanadatos, Jurásico, Patagonia.

INTRODUCTION

The San Roque project is located in the eastern sector of the North Patagonian Massif, in Río Negro province, Argentina (Fig. 1a, b). It is an epithermal and polymetallic deposit (Dill et

al. 2013a, Jovic et al. 2015, Padelletti Di Marco 2023) that covers an area of approximately 74,000 hectares. It is characterized by epithermal manifestations that occur as quartz and sulfide veins, veinlets, and stockworks with strong structural control. Geochemical exploration by mining companies revealed that the sulphide-rich epithermal mineralization shows relatively high levels of Au, Ag, Zn, Pb, Mo and In. One of the most interesting elements, in view of the economic potential (in addition to the Au and Ag contents), is the presence of In, which registers concentrations up to 1,500 ppm in hypogenic ore and almost 15,000 ppm in the supergene zone (Falls and Montgomery 2012). Currently, the available data for deposits with In which are affected by supergene processes is particularly limited and the San Roque project is not the exception, since until now there has not been a suitable study with the characterization of the mineral phases that concentrate economically important metals (In, Pb, Ag, Zn, Mo, Cu, Au) in the supergene zone. Although these metals are not critical elements in Argentina, they can be considered of strategic economic importance due to their critical nature worldwide (USA, European Union, China, United Kingdom), which ultimately indicates the importance attached to them for the industry promoting their exploration and eventual economic use (Zappettini 2021).

Supergene deposits are the subject of increasing interest for mining industries, driven by an increasing demand for metallic elements for new technologies. In this context, the near-surface location and the weathered and easily exploitable host rocks, are advantages over hypogene mineralization due to their relatively easy and rapid accessibility and extraction (Verhaert et al. 2020 and references therein). An additional benefit of secondary ores is their higher metal content, compared to primary sulfides (Sillitoe 2005), although their complex mineralogy can also represent a challenge for ore processing. Supergene minerals formed through these processes and their stability in exogenous settings play a key role in mobility of chemical elements of economic importance. For this reason, the study of these minerals contributes to elucidate mechanism of metals transport and accumulation under natural conditions. Also, it contributes to a better understanding of the geochemical behavior of In –

among others metals - in near-surface portions of the Earth's crust. This stands for more than relevant information for exploration and explotation of metals in this region of Argentina.

Within the San Roque project, Del Indio Structure is one of the most explored epithermal structure, it has a general NE-SW strike and a length of 300 m (Fig. 1b). The supergene zone is best represented along this structure, since a complex weathering profile incorporating part of the orebody was described. This paper documents a detailed study of newly collected samples belonging to the In-rich oxidation zone in Del Indio Structure, where the supergene mineral associations are described and semicuantitative mineral compositions are presented. In addition, we also characterize the epiclastic host-rocks of the mineral associations and the interpretation of strategic metals.

GEOLOGY OF THE SAN ROQUE PROJECT

The San Roque polymetallic (Au-Ag-Cu-Pb-Zn) project is characterized by quartz and sulfides veins, veinlets and stockworks of quartz and sulfides with epithermal features, containing critical metals such as In, Mo, Ga (Dill et al. 2013a; Jovic et al. 2015, Padelletti Di Marco et al. 2023). They are mainly hosted in acidic volcanic and epiclastic rocks of jurassic age belonging to the Marifil Volcanic Complex (Cortés 1981, Dill et al. 2013a) and locally, in the paleozoic metamorphic basement of the Nahuel Niyeu Formation (Greco et al. 2015; Fig. 1a, b).

The studied area comprises a volcano-sedimentary basin (~2 km-diameter) bounded by foliated metasediments of the metamorphic basement rocks (Nahuel Niyeu Fm.). Overlying the metamorphic rocks is a relatively flat lying represented by volcanoclastic matrix- and clast-supported breccias and conglomerates, coarse to fine grain sandstones and siltstones. Besides, volcanic pyroclastic and coherent facies are interbedded with reworked epiclastic facies. In addition, subvolcanic facies of high-level trachyte and rhyolite porphyry stocks intrude the basement rocks and the volcano-sedimentary sequence. The latter represents an

active volcanism coeval with volcanoclastic sedimentation attributed to the Marifil Volcanic Complex (Pankhurst et al. 2000, Martinez et al. 2001); (Fig. 1a, b).

Locally, fossiliferous marine sedimentary rocks of the overlying cretaceous to paleocene Arroyo Barbudo Formation are exposed (Fig. 1a). Tertiary basaltic flows of the Somuncurá Formation built up an extensive plateau cropping out southward the San Roque project near the Aguada Cecilio town (Fig. 1a). According to Kay et al. (2007), the basaltic flows were extruded in an intraplate setting during an extensional processes linked to a local thermal instability of the mantle. The effusions developed mainly in the Oligocene (33 to 26 Ma), although the available ages cover a wide temporal range (Ardolino et al. 1981, Cordenons et al. 2020). In the northeast of the San Roque project, miocene-oligocene marine sedimentary rocks of the Gran Bajo del Gualicho Formation, continental sandstones of the Río Negro Formation and polymictic conglomerates corresponding to the "*rodados patagónicos*" unit are exposed (Fig.1a). Holocene is represented by alluvial and colluvial deposits (Martinez et al. 2001; Fig. 1a, b).

A series of northeast and northwest trending faults have been interpreted from surface topography, geophysical data, geological mapping and drillcore intersections (Fig. 1b). These faults are thought to control the extent of the half-graben basin, the hydrothermal activity, as well as the porphyritic intrusions. Field relationships interpreted from drilling and mapping strongly suggest that faulting and hydrothermal activity responsible for veining and mineralization were broadly contemporaneous (Falls and Montgomery 2012).

Epithermal polymetallic hypogenic mineralization in Del Indio structure

Based on hydrothermal breccias and veins characteristics, fill textures, quartz-sericitic alteration, Fe-poor sphalerite with fluid inclusions homogenization temperatures (215º to 248 ºC, Gómez et al. 2008; 243 to 273 ºC, Padelletti Di Marco et al. 2023), low to moderate salinity of the fluids (4.7 to 6.5%NaCl eq. Gómez et al. 2008; 5.11 to 5.57%NaCl eq. Padelletti Di Marco et al. 2023), mineralization was defined as an epithermal system of low to

intermediate sulfidation. Ore mineralogy consists in native gold, sphalerite, galena, chalcopyrite, and minor amounts of others Cu-sulfides and sulfosalts, while gangue minerals mainly comprise quartz, with subordinate calcite and fluorite (Gómez et al. 2008, Dill et al. 2013a, Padelletti Di Marco et al. 2023). According to the hydrothermal alteration that occurred in detrital and magmatic Al-bearing minerals, and the development of illite >> kaolinite ± chlorite as patches or pervasive alteration in the rocks, as well as voids and cracks filling, it was interpret that the hydrothermal fluids followed feeders and conduits, and also they diffused in the pores of the host volcanoclastic and epiclastic rocks, resulting in a hydrothermal assemblage with very low acid buffering capacity (Padelletti Di Marco 2023).

The hypogenic polymetallic mineralization in Del Indio structure occurs as veinlets, stockworks and locally hydrothermal breccias in intervals of variable thickness (apparent thickness 7 to 20 m) hosted in the volcaniclastic sequence (Fig. 2 a, b). The hydrothermal veins and veinlets are between 0.5 and 5 cm thick while the brecciated sectors have an apparent thickness of up to 10 cm. The veinlets are continuous, with sharp edges, generally lack internal symmetry and show alteration halos in the host rocks. The syn-mineralization episode is characterized by the precipitation of two generations of sphalerite: banded sphalerite (Sp 1) and colloform sphalerite (Sp 2) associated with pyrite, chalcopyrite and galena (Fig. 2c). Edges of chalcopyrite crystals are usually replaced by bornite, covellite, anilite, or tetrahedrite group minerals. Quartz, carbonates and fluorite precipitated as late filing of the cavities during the post-mineralization episode (Padelletti Di Marco et al. 2023).

SAMPLING AND ANALYTICAL METHODS

In the field, a detailed sampling of the cores of two drillholes (MF-DDH-02: 3516788E, 5487020N and MF-DDH-04: 3516736E, 5486975N) that intercepted Del Indio structure at different depths was carried out. The drill holes have a NW-SE orientation, an inclination of -60° and depths of 105 and 120 m, respectively (Figs. 1b, 2a, b). Based on geochemical

information provided by Marifil Mines S.A. mining company, sampling was focused on intervals with anomalous metals contents.

Rock samples from the selected drillholes were analyzed for 41 elements at the Alex Stewart laboratory in Mendoza using four-acid digestion and emission spectrometry (ICP-ES). A statistical analysis of the geochemical data was carried out by estimating the Pearson correlation coefficient (r), as a quantitative method to determine the degree of correlation between the analyzed elements. Ranges were established to define low (r = 0.1 - 0.4), moderate (r = 0.4 - 0.7), high (r = 0.7 - 0.9) and perfect (r = 0.9 - 1) positive correlations. Box and whisker plots were performed in order to identify the chemical elements with anomalous contents. Then, based on these results, the anomalous elements were selected to make the lithogeochemical profiles.

A total number of 13 thin and polished sections of representative rock-samples were prepared in the Petrotomy Laboratory of the INGEOSUR, CCT CONICET Bahía Blanca and were analyzed with a Nikon Eclipse E600 petrochalcographic microscope. A JEOL JSM 35 CP scanning electron microscopy (SEM), equipped with an energy dispersive X-ray spectroscop detector (EDS) belonging to the CCT-CONICET Bahía Blanca was used to analyze the chemical composition of the mineral phases in 7 representative petrochalcographic samples and rock fragments. In addition, compositional maps were performed in the analyzed samples in order to show the distribution of chemical elements in each mineralogical phase of interest.

RESULTS

Host rocks of supergene polymetallic mineralization

The studied drillholes from Del Indio Structure intercepted a succession of epiclastic facies interbedded with volcaniclastic facies from the Marifil Volcanic Complex. The lithological characteristics and the size of the fragments in the epiclastic facies allowed to define two

211 subfacies as the principal rocks in the supergene zone: a) polymictic orthobreccia and, b)
212 mudstone (Fig. 2a, b, d, e).
213 The polymictic orthobreccia is light gray or dark green in color at greater depths (Fig. 2c),
214 while at shallower depth it is pinkish-brown in color (Fig. 2d). It has a matrix-supported to
215 clast-supported texture, where the clastic fraction constitutes 10 to 60% by volume (% vol.) of
216 the rock. The lithoclasts are angular to rounded with sizes between 0.2 and 5 cm and they
217 predominantly correspond to acid volcanic rocks with a porphyric texture and aphanitic
218 groundmass (up to 35%). Subordinately, smaller lithoclasts (maximum 0.5 cm) of pelitic
219 rocks and foliated metamorphic rocks can be distinguished (Fig. 2c, d). Locally, idiomorphic
220 to hypidiomorphic clasts of quartz (2 to 10 % vol.) and feldspar (3 % vol.) can be
221 distinguished with sizes that may vary between 400 and 800 µm (Fig. 2c, d), the latter
222 partially or totally replaced by illite >> kaolinite < chlorite. The matrix (25 to 75 % vol.) is fine
223 to medium sand size and includes the same components mentioned previously. Besides up
224 to 15% ferruginous cement can be distinguished (Fig. 2c, d).
225 The mudstone subfacies was intersected throughout the drillhole and occurs as interbedded
226 levels between the coarse-grained lithologies (Fig. 2e). They present a massive to finely
227 laminated fabric with greenish-gray, dark brown and grey color, and no evidence of
228 bioturbation. The clasts may vary in grain-size from clay (~1.5 µm) to coarse silt (~50 µm)
229 and are mainly composed of quartz, feldspars, illite, and disseminated framboidal pyrite.
230 At the contacts between the two different lithologies of the epiclastic facies, a higher
231 concentration of iron oxides veinlets is observed.
232
233 **Whole-rock geochemistry**
234
235 With the aim of determining the distribution and/or variation in concentration of chemical
236 elements, box-and-whisker plots were constructed (Appendix A; Fig. 3) in order to define
237 which of them show chemical outliers along the oxidation zone. Bulk-ore metals grades show
238 a wide range in concentration, as shown in diagrams in figure 3. In general metals show a

high dispersion with a positively skewed asymmetric distribution; while Fe and Mn show a more symmetric distribution.

Rock sample descriptions and analyses of the lithogeochemical profiles in the studied drillholes indicate a complex chemical weathering profile that reaches a current depth of 45 and 48 m in MF-DDH-02 and MF-DDH-04 drillholes, respectively (Fig. 4a, b). In both drillholes the oxidation zone includes Del Indio structure, which represents the high-grade zone.

In MF-DDH-02 drillhole (Fig. 4a), the oxidation zone contains the highest concentrations of Fe (8.06 wt.%), Mn (>2 wt.%), Zn (7786 ppm), Pb (5705 ppm), Cu (3013 ppm), In (2435 ppm), V (1917 ppm), As (609 ppm), P (607 ppm), Sr (333 ppm), Mo (241 ppm), Ga (15 ppm), Ag (5.6 ppm), Au (3.65 ppm). Below the oxidation level, the Cu, In, V, As, Sr, Mo, Bi, Ga, Ag, Au contents are very low, sometimes below the limit detection, which agrees with the scarcity of hydrothermal veins described in the transitional and hipogenic zones.. Fe, Zn and Pb present variable concentrations below the oxidation level with maximum values in those samples that present hydrothermal veins and veinlets. Sulfur and Cd have similar geochemical profiles, both elements are scarce to undetectable throught the oxidation zone and show a sharp increase in their concentrations below it.

In MF-DDH-04 drillhole the highest contents of Fe (7.24 wt.%), Mn (> 2 wt.%), Pb (5530 ppm), V (1857 ppm), As (633 ppm), P (816 ppm), Sr (270 ppm), Mo (227 ppm) and Au (7.2 ppm) are in the oxidation zone (Fig. 4b). Besides, the highest concentrations of Ag (31.3 ppm), Cu (1290 ppm) and In (780 ppm) are associated with Del Indio Structure intercepted between 42.6 and 46.3 m depth; Zn, Cd and Ga present low to undetectable concentrations (0.21 wt.%, 6 ppm and 15 ppm, respectively). Below the oxidation level (from 48 m to the end of the drillhole; Fig. 3), the highest contents of Zn (2.55 to 14.81 wt.%), S (4.24 to 9 wt.%), Cu (578 to 4490 ppm), In (206 to 1160 ppm), Cd (154 to 888 ppm), Ga (< 65 ppm) and Ag (6.7 to 60.7 ppm) are also present. These elements are preferentially concentrated in a sector intercepted at a depth of 74 m, with an apparent thickness of 4.5 m, and which

corresponds to an interval with abundant veins and irregular veinlets filled by representative sulfides of the hypogene zone (Fig. 2c).

Pearson's correlation coefficients were calculated with the geochemical data of all samples above the oxidation level (Appendix A). In MF-DDH-02 drillhole, the Pearson correlation coefficients indicate several perfect positive correlations, among which are highlighted: In - Bi (r = 0.99), In - V (r = 0.93), As - Mo (r = 0.96), As – Cu (r = 0.93), Cu – Mo (r = 0.96) and V - Bi (r = 0.91). In the MF-DDH-04 drillhole there are also numerous perfect positive correlations: Ag - Cu (r = 0.98), Ag - Mo (r = 0.93), As - Au (r = 0.93), As - In (r = 0.97), As - Mo (r = 0.92), As - V (r = 0.91), Au - Bi (r = 0.95), Au - In (r = 0.97), Bi - In (r = 0.93) and Cu - Mo (r = 0.93).

Supergene mineralogy in the oxidation zone

Above the oxidation level the supergene alteration zone was recognized (Fig. 4a, b). This zone is characterized by a supergene mineral-association that may occur: a) as fine-grained aggregates that fill dissolution cavities and microfractures in the polymictic orthobrecccia, b) replacing hypogenic minerals in quartz vein/veinlets and c) forming patchy aggregates in the finer grained rocks (Fig. 2). The recognized minerals containing anomalies in In and other metals of economic interest are described below in decreasing order of abundance (Fig. 5).

Hematite: is a moderately abundant to abundant mineral that is present in most samples along the supergene zone. It occurs as patches, cavity and microfractures fillings, and as sulfide replacement (Fig. 5a-c). Hematite and Fe oxy-hydroxides stain veins and veinlets filled with quartz and sulfides (mainly pyrite) with a reddish color. The presence of empty spaces and cavities resulting from the dissolution of primary sulfides is common (Fig. 5a). Under the microscope, crystalline aggregates are fine-grained and have massive, skeletal, fibrous, spherical, botryoidal and mammillary habits with banded texture, where the bands have a thickness that varies between 10 and 250 µm (Figs. 6). In some cases, iIdiomorphic crystals of pyrite are partially to totally pseudomorphcally replaced by hematite (Fig. 5c). The

semi-quantitative chemical analyses carried out on hematite crystals (n = 27; Appendix B, table 1), together with images of backscattered electrons with distribution of concentrations of chemical elements (chemical maps), allowed to determine that this mineral concentrates in addition to Fe (35.4-60.4 wt.%), other metallic elements such as Pb (up to – 11.3 wt.%), V (up to. - 2.5 wt.%), Cu (up to – 2.5 wt.%), Zn (up to – 1.7 wt.%), As (up to – 1.7 wt%), In (up to - 1.3 wt.%), Mn (up to 0.9 wt.%) (Fig. 6).

Manganese oxides: are also widely distributed along the supergenic zone. Macroscopically they are observed as dense, massive, black to black-brown aggregates in oxidized ore samples, closely associated with quartz veins and veinlets and with hematite and/or Fe-oxy-hydroxides (Fig. 5d). Using the polarizing microscope with reflected light they occur as common fine-grained colloform aggregates with light and dark bands showing different shades of gray (Fig. 5e). Coronadite, ideally $Pb(Mn^{4+}_6,Mn^{3+}_2)O_{16}$ belongs to the coronadite group, and the hollandite supergroup, itwas found in samples from drillcore MF-DDH-04. Coronadite fills vugs in quartz veinlets and occurs as botryoidal aggregates with a rough appearance (Fig. 5f). Manganese and Pb contents may vary between 30.4 to 55.9 wt.% and 16.8 to 28.5 wt.%, respectively (n = 13, Appendix B, table 2). It contains accessory amounts of Cu (0.9 – 2.58 wt%), V (1.3 – 2 wt.%, and only minor contents of Al, Si. Some analyses (n = 3) registered Fe contents (6.7 to 11.1 wt.%), and this could be attributed to the presence of ferricoronadite $Pb(Mn^{4+}_6Fe^{3+}_2)O_{16}$ (Chukanov et al. 2016).

Mottramite: ideally $PbCu(VO_4)(OH)$, belongs to the adelite-descloizite group, a large group of minerals of the general form $AB(XO_4)(Z)$, which contains intermediate-size divalent cations (Ca and Pb) at the A site, divalent transition metals (Cu, Zn, Fe, Mn, Mg, Co and Ni) in site B. X represents the structural site for elements such as P, As^{5+} and V^{5+} and Z represents the structural site for OH, F, Cl (Richmond 1940). Although mottramite is not an abundant mineral, it was identified in most of the studied samples along the supergenic zone. This vanadate occurs as fine-grained (< 60 μm) late idiomorphic fibrous or prismatic crystals that grow on colloform hematite aggregates (Fig. 6), and inlate cavities within totally or partially pseudomorphically replaced pyrite crystals (Fig 5g, h). Locally, mottramite occurs as

colloform aggregates that fill microfractures (Fig. 5h) and cavities in volcanoclastics rocks (Fig. 5i). It is transparent to subtranslucent with a variable green to yellow color with slight pleochroism. Lead is the dominant cation at the A site (47.2 to 57.4 wt.%, n = 8). B site is predominantly occupied by Cu (6.7–13 wt.%). Vanadium is the dominant chemical element at the X site (10.2 to 12.1 wt.%). Iron, Zn, and Mn are also present with maximum values of (10.2; 5.5 and 1 wt.%, respectively; Appendix B, table 3). From the chemical map images and EDS analysis it is possible to observe that mottramite concentrates minor amounts of In, Ga, P and Cl, the latter two, probably occupying X and Z sites, respectively (Fig. 6i-l).

Plumbojarosite: $Pb_{0.5}Fe^{3+}_3(SO_4)_2(OH)_6$ is a relatively scarce mineral in samples from the supergenic zone, but, in all the studied samples is always associated with Fe-oxi-hydroxides (Fig. 2f, Fig. 5j, k). It occurs as fine-grained (< 1 mm) crystalline aggregates with a radial fibrous habit closely associated with pyrite oxidation, forming anhedral grains around pyrite crystals and intergrown with hematite (Fig. 5k). Under the polarizing microscope with transmitted light are reddish-brown in color, with weak pleochroism. From the semi-quantitative chemical analyses (n = 8; Appendix B, table 4) it was determined that the Pb content varies between 5.8 and 11.5wt.%, while Fe and S concentrations vary between 14.5 to 23.1 wt.% and 5.7 to 8.4 wt.%, respectively. The subordinate participation of K (1.2 - 2.2 wt.%), As (0.7 - 1.2 wt.%) and In (up to - 0.4 wt.%) was also determined (Fig. 7).

DISCUSION

In the San Roque project, the mineralogical, textural, and chemical characteristics of the supergene minerals described in this contribution provide strong evidence for an origin from oxidation of hypogenic polymetallic mineralization, partial mobilization of chemical elements, and open space re-precipitation, as well as *in situ* replacements (e.g. pseudomorphic hematite after pyrite leaving only relics cores of that mineral). The presence of an oxidizing environment and fluids leaching the primary ore are the main factors leading to the formation of supergene ores (Choulet et al. 2014, Boni y Mondillo 2015, Verhaert et al. 2017, Sillitoe

2019). Other factors that may have played a role in the formation of the supergene zone in the San Roque project include uplifting of the area and fracturing with exhumation and subsequent weathering of host rocks and increasing climatic aridity, or a combination of all these. In San Roque area, the exhumation process happened after the Jurassic (Martinez et al. 2001), and an increase in aridity as a product of the uplift of the Patagonian Andes, would have depressed the regional water tables, facilitating the oxidation of primary minerals and the formation of supergene minerals such as those documented in this contribution.

The importance of the porosity and the permeability of the host rocks, together with the structural control evidenced by the presence of faults/fractures may facilitate the percolation of meteoric waters since they represent main controls for the circulation of supergene fluid flows (Sillitoe 2019). This was evidenced in this study, since according to the distributions of the chemical elements along the volcano-sedimentary columns intercepted by the studied drillholes (Fig. 4), the highest concentrations of metals were found in the epiclastic levels of coarser granulometry, associated with fault and/or fractures zones.

Another factor that favored the formation of the supergene minerals described here is related to the mineralogy of the host rocks. The epiclastic rocks described in this contribution are mostly composed of clasts of volcanic origin characterized by an acidic mineral association with abundant quartz, K-feldspars relicts and secondary minerals such as illite, minor kaolinite and traces of chlorite, and also fragments of the metamorphic basement rocks, providing a final association with very low acid buffering capacity.

Supergene metal deposits contribute significantly to the world's supply of selected base metals (Cu, Zn, Ni, Co) and structural metals (Al, Fe, Ni, V, Reich and Vasconcelos 2015). Zones of supergene sulfide oxidation are widely developed at several Au-Ag epithermal deposits in the Deseado auroargentiferous province, Deseado Massif located in Patagonia, Argentina (Schalamuk et al. 1997; Fernández et al. 2008; Sillitoe 2019), and had influenced the increase of metal grades (e.g Mina Marta, Páez et al. 2016; veta Eureka West, Cerro Negro project, Permuy Vidal 2014; Veta Julia, Virginia project, Luna 2021). In the San Roque project, the hypogenic minerals that contain In are sphalerite >> roquesita and Cu-sulfides

and sulfosalts, while in the supergene zone only dzhalindite $In(OH)_3$ was described (Dill et al. 2013a). According to observations with SEM and semi-quantitative analyses of the San Roque project studied samples, the main supergene minerals that concentrate In are attributed to hematite, plumbojarosite and mottramite.

Semi-quantitative analyses on hematite crystals revealed very variable Fe contents (35.4-60.4 wt.%), together with the presence of other metallic elements such as In, V, Cu, Zn, Pb. This provides evidence of the ability of this mineral to trap and/or assimilate metals during its formation by replacement of the primary ore, mainly pyrite, at room temperature and near-neutral pH (Wood and Samson 2006). It has been proposed that the metal retention capacity of hematite and other Fe-oxi-hydroxides could have been enhanced by the presence of sulfates in the depositional environment (Swedlund et al. 2009). Hematite and Fe-oxy-hydroxides with In and Ga contents, among others, were described in the oxidized ores of the Kabwe Zn-Pb deposit (formerly known as 'Broken Hill'), located in central Zambia (Mondillo et al. 2018). These authors proposed that during the last stage of supergene alteration of sulfides, the more immobile In and Ga were residually incorporated into the newly formed Fe-oxy-hydroxides.

Mottramite is a vanadate typically found in oxidized zones of vanadium bearing supergene deposits, but may also be abundant within and/or around Cu, Pb, Zn sulfides ores (Yans et al. 2017 and references therein). It forms at low temperatures (40-50°C), in arid, acidic and slightly reduced environments, such as the boundary between the phreatic and vadose zones (Boni et al. 2007). However, Dill et al. (2013b) suggested that vanadates are most stable under strongly oxidizing and neutral pH conditions. The association of mottramite, hematite and Fe-Mn-oxy-hydroxides at the San Roque project implies that the hypothesis of Dill et al. (2013b) is more adequate in this case, and it was also proposed for other polymetallic deposits with supergene alteration and mottramite formation (Verhaert et al. 2020). The occurrence of mottramite irregularly scattered in the studied samples from the supergene zone of Del Indio Structure as microveinlets /microfractures crosscutting the oxidized mineralization (Fig. 5h), overgrowing walls of cavities in skeletal hematite (Fig. 5c,

406 g), precipitating with late colloform/botryoidal hematite aggregates (Fig. 6), corroborates the
407 observation of Boni et al. (2007) and Verhaert et al. (2020) that vanadates such as
408 mottramite often form during late phases in the supergene history.
409 Schwellnus (1945), Verwoerd (1953), van der Westhuizen et al. (1989), and Boni et al.
410 (2007), proposed that mottramite forms by recombination of V mobilized from host rocks
411 and/or sulfides, with residual Cu and Pb amounts deriving from primary sulfides. In
412 Patagonia, mottramite was described in a kaolin deposit located in the southeast of Los
413 Menucos town (Marfil et al. 2002). These authors suggest that vanadium mobilized from
414 hydrothermally altered rhyolitic tuffs of the Sierra Colorada Formation, whose vanadium
415 content is ~ 100 ppm, precipitated as isolated crystals directly related to alunite from
416 hydrothermal solutions or acid hot springs. The hypogenic ore in the San Roque project is
417 not enriched in V, as well as the host rocks below the oxidation level (Fig. 4). For this reason,
418 considering the relatives V contents in the rocks of the region, and their proximity to the San
419 Roque project area (Fig. 8), it is shown that all the volcanic units of the Meseta de
420 Somuncurá have high contents of V (specially those with trachybasalt, basaltic
421 trachyandesite or basaltic-andesite lithologies), therefore, they may be the main source of V
422 for this region. Since the tertiary lava-flows of the Somuncurá Formation are widely extended
423 in the Río Negro province and they are the closest to the San Roque project located
424 southward of the project area (Fig. 1a) we suggest that this formation can be the main
425 possible source of V. In this sense, Reimann and de Caritat (2012) mentioned that basaltic
426 rocks show, in fact, the highest V concentrations among the most diffused crustal rock types.
427 This is also the case for the lithologies in the surroundings of San Roque project (Fig. 8).
428 Finally, the peculiar V concentrations in the supergene zone in San Roque project is also
429 favored by their chemical-physical conditions, since V according to Wright and Belitz (2010)
430 is highly mobile in oxidized and alkaline conditions. In this way, the vanadate's formation in
431 the San Roque project would have occurred during or after basalts extrusion which began to
432 be extruded during the early Oligocene (Cordenons et al. 2020 and references there in).

In the studied samples, plumbojarosite has a local distribution and occurs as patches and replacements in the host rock, associated with Fe-Mn-oxy-hydroxides and hematite. The presence of plumbojarosite indicates high concentration of Pb available in the system, low pH environments, it generally represents mature Pb phases, and was described in the supergene oxidized zone of Pb-Zn deposits (Scott 1987, Davis et al. 1993, Basciano and Peterson 2010). Plumbojarosite was not observed as cavity infillings indicating their formation was not by direct precipitation from weathering solutions, for this reason, its formation is inferred to the related replacement in situ of unstable hypogene minerals under an oxidizing environment, such as sulfides. This would also explains the In contents observed in this mineral, since sulfate complexes and metal ions involved in sulfates precipitation are originated from the hypogenic sulfides, whereas Na and Al most probably derived from silicates of the host rocks.

These results, among others described in other deposits from Patagonia and the world (e.g. Moura et al. 2007, López et al. 2015), show that In behaves as an immobile metallic element under oxidizing conditions. The stability of In in the supergene zone was explained by the extremely low solubility of this element at pH values between ~4.5 and ~9, and in a low temperature range (Ogawa et al. 2012; Schwarz-Schampera and Herzig, 2002).

Coronadite usually occurs as a primary mineral in hydrothermal veins or can crystallized from hot springs, also might be of secondary origin in oxidized zones above the manganese-bearing rocks or can be found in bedded sedimentary deposits (Vlasáč et al. 2021). In this contribution, coronadite most likely has a secondary origin due to their textural features and mineral association described in all samples. In turn, the low Mn contents present in the samples located in deeper zones, below the supergene oxidation zone (Fig. 4), indicate that the primary sulfides and host rocks are not enriched in this element.

Neither Au, Ag nor electrum were identified in the studied samples. Likewise, these metals were not detected as inclusions or as trace elements in other minerals based on the analytical techniques used in this research. Nonetheless, their presence was confirmed in the whole-rock geochemical analyses provided by the mining company (Figs. 3, 4). On the

other hand, among the cavities of the Fe-oxy-hydroxides of rock samples from the MF-DDH-04 drillhole (sample 7469; 44 m depth, Au: 7.2 ppm), abundant small crystals (10 to 25 μm), with yellow to silver colors and high reflectance, have been observed. Some of them, have been individualized as gold and/or electrum grains (Guido and Jovic 2007; in a private report prepared for Marifil Mines S.A). Also, it is important to note that in the studied supergene zone, Au and In show a perfect positive geochemical correlation (Appendix A). In turn, these elements also have perfect and high positive correlations with Ag, As, Cu, Mo, V, Bi and Sn, which suggests that they could be used as guide elements for the exploration of both metals. Probably, during the early stages of the supergene alteration, the mineralogy of the host volcaniclastic succession combined with the veinlet/stockwork/disseminated style of mineralization of hypogene minerals and the high potential of pyrite to produce highly oxidizing agents (Plumlee 1999), enhanced oxidation process resulting in liberation of microparticulate Au. Gold, could also have been mobilized with chloride complexes that can occur in arid supergenic environments (Reich and Vasconcelos 2015).

CONCLUSIONS

In the San Roque project, a supergene alteration process have affected the upper portion of the epithermal mineralization, hosted in the polymictic orthobrecha epiclastic subfacies form the Marifil Volcanic Complex. The porosity and the permeability of the host rocks, together with the structural control with the presence of faults/fractures, facilitate the percolation of meteoric waters, and therefore, the supergene fluids flow. Rock heterogeneity between the mudstones and the coarsed grained polymictic orthobreccia played a critical role in the development of the supergene mineralization. The veinlets, stockwork and, in a lesser extent, disseminated mineralization style of the hypogenic ore, with In-bearing-sphalerite and pyrite as the predominant sulfides, combined with the porosity and limited acid-buffering capacity of the polymictic orthobreccia, favored the penetration of slightly acidic, oxidizing and relatively V-rich meteoric waters and the subsequent oxidation process. Hematite and

Fe-Mn-oxy-hydroxides predominate at the uppermost part of the deposit, whereas secondary minerals as mottramite and plumbojarosite are present in minor amounts. These supergene minerals concentrate metals of strategic economic importance such as In, Pb, Cu, V, Mo, which behaved immobile in this oxidizing environment.

The peculiar V concentration in the supergene zone in San Roque project was favored by their chemical-physical conditions, since V is highly mobile in oxidized and alkaline conditions. The V source is related with the Somún Curá Magmatic Province, especially with the Somuncurá Formation, therefore, vanadates in the San Roque project must have formedduring or after early Oligocene.

Despite the perfect positive geochemical correlation between In and Au in the supergene zone represented in the studied drillholes and notwithstanding the fact that Au and/or electrum grains have been already identified in other locations of the San Roque project, they were not found in the studied samples of the supergene zones represented in both drillholes that intercepted Del Indio Structure. This absence may be related with the highly oxidizing environment that enhanced the liberation of Au microparticles and mobilized Au with chloride complexes common in arid supergenic systems.

ACKNOWLEDGMENTS

The authors thank the Department of Geology of the Universidad Nacional del Sur for having financed part of the material necessary to carry out this contribution. Likewise, this work was financed through the project 24/H148 of the Secretaría General de Ciencia y Tecnología de la Universidad Nacional del Sur (SGCyT - UNS), granted to Dr. G. Ferracutti. A special thanks to the Marifil Mines S.A. mining company and to the geologists Lic. Dick Walters, Daniel Buffone and Enzo Bonuccelli for making available not only the drillcore samples and the geochemical information from the San Roque project to us; but also for financing the studies carried out with SEM in the representative samples.

REFERENCES

Ardolino, A. 1981. El vulcanismo Cenozoico del borde suroriental de la meseta de Somún Curá. Actas 8º Congreso Geológico Argentino, 3: 7-23. Buenos Aires.

Asiain, L.M., Ferracutti, G., Gargiulo, M.F., Bjerg, E.A. and Hauzenberger, Ch. 2021. Petrología y geoquímica de basaltos alcalinos de diques y conos ubicados en el bajo de El Caín, Meseta de Somuncurá. Revista de la Asociación Geológica Argentina 78(2): 246-267.

Asiain, L., Gargiulo, M.F., Bjerg, E.A., Ntaflos, Th. and Reitinger, J. 2019. Petrografía y geoquímica de traquibasaltos y traquiandesitas basálticas de las Vulcanitas Corona Chico y del Complejo Volcánico Barril Niyeu, noroeste de la Meseta de Somuncurá, provincia de Río Negro. Revista de la Asociación Geológica Argentina 76(1): 08-23.

Asiain, L., Gargiulo, M.F., Reitinger, J., Ntaflos, Th. and Bjerg, E.A. 2017. Petrografía y geoquímica de lavas básicas del sector noroeste de la Meseta de Somuncurá, provincia de Río Negro. Revista de la Asociación Geológica Argentina 74(4): 570-582.

Basciano L.C. and Peterson, R.C. 2010. A crystallographic study of the incomplete solid-solution between plumbojarosite and jarosite. The Canadian Mineralogist 48: 651-659.

Boni, M. and Mondillo, M. 2015. The “Calamines” and the “Others”: The great family of supergene nonsulfide zinc ore. Ore Geology Reviews 67: 208-233.

Boni, M., Terracciano, R., Evans, N.J., Laukamp, C., Schneider, J., Bechstadt, T. and Bechstadt, T. 2007. Genesis of vanadium ores in the Otavi Mountainland, Namibia: Economic Geology 102: 441-469.

Choulet, F., Charles, N., Barbanson, L., Branquet, Y., Sizaret, S., Aomar, E., Badra, L. and Chen, Y. 2014. Non-sulfide zinc deposits of the Moroccan High Atlas: Multi-scale characterization. Ore Geology Reviews 56: 115-140.

Chukanov, N.V., Aksenov, S.M., Jančev, S., Pekov, I.V., Göttlicher, J., Polekhovsky, Y.S., Vyacheslav S. R., Yuliya V. N and Van, K.V. 2016. A new mineral species ferricoronadite, Pb $[Mn_6{}^{4+}(Fe^{3+}, Mn^{3+})_2]O_{16}$: mineralogical characterization, crystal chemistry and physical properties. Physics and Chemistry of Minerals 43: 503-514.

545 Cordenons, P. D., Remesal, M. B., Salani, F. M. and Cerredo, M. E. 2020. Temporal and
546 spatial evolution of the Somún Curá magmatic province, northern extra-andean Patagonia,
547 Argentina. Journal of South American Earth Sciences 104:102881.
548 Cortés, J. 1981. El sustrato precretácico del extremo nordeste de la provincia del Chubut.
549 Revista de la Asociación Geológica Argentina 36(5): 217-235.
550 Davis, A., Drexler, J.W., Ruby, M.V. and Nicholson, A. 1993. Micromineralogy of mine
551 wastes in relation to lead bioavailability, Butte, Montana. Environmental Science and
552 Technology 27: 1415-1425.
553 Dill, H.G., Garrido, M.M., Melcher, F., Gomez, M., Weber, B., Luna, L. and Bahr, A. 2013a.
554 Sulfidic and non-sulfidic indium mineralization of the epithermal Au–Cu–Zn–Pb–Ag deposit
555 San Roque (Provincia Río Negro, SE Argentina) with special reference to the “indium
556 window” in zinc sulfide. Ore Geology Reviews 51: 103-128.
557 Dill, H.G., Techmer, A. and Botz, R. 2013b. Copper-bearing encrustations: A tool for age
558 dating and constraining the physical-chemical regime during the late Quaternary in the Wadi
559 Araba, southern Jordan. International Journal of Earth Sciences 102: 1541-1561.
560 Falls, R. and Montgomery, A. 2012. Report on the 2010-2011 Diamond Drilling, Geophysical
561 and Geochemical Exploration Program on the San Roque Property. Prepared for NovaGold
562 Resources Inc. 264 pp.
563 Fernández, R. R., Blesa, A., Moreira, P., Echeveste, H., Mykietiuk, K., Andrada de Palomera,
564 P. and Tessone, M. 2008. Los depósitos de oro y plata vinculados al magmatismo jurásico
565 de la Patagonia: revisión y perspectivas para la exploración. Revista de la Asociación
566 Geológica
567 Argentina 63(4):665-681.
568 Ferracutti, G.R., Asiain, L., Bjerg, E.A., Gargiulo, M.F., Hauser, N. and Hauzenberger, Ch.
569 2022. Cuerpos traquíticos del Bajo de El Caín, Meseta de Somuncurá, Provincia de Río
570 Negro, Patagonia Argentina. Revista de la Asociación Geológica Argentina 79(2): 292-314.
571 Gómez, C., Luna, L., Garrido, M. y Bonuccelli, R. 2008. Manifestación de indio en el
572 Macizo Nordpatagónico: proyecto San Roque, provincia de Rio Negro. 9°

573 Congreso de Mineralogía y Metalogenia: 125-128.
574 Greco, G.A., González, P.D., González, S.N., Sato, A.M., Basei, M.A., Tassinari, C.C. y
575 Llambías, E.J. 2015. Geology, structure and age of the Nahuel Niyeu formation in the
576 Aguada Cecilio area, North Patagonian Massif, Argentina. Journal of South American Earth
577 Sciences 62: 12-32.
578 Guido, D. and Jovic, S. 2007. Informe del estudio de secciones pulidas en testigos de
579 perforación de la empresa MARIFIL S.A. Private report 9 pp.
580 Jovic, S., López, L., Guido, D., Redigonda, J., Páez, G. y Ruiz, R. 2015. Indium
581 mineralization in epithermal polymetallic deposits of Patagonia Argentina. In: Mineral
582 Resources in a Sustainable World 13th SGA Biennial Meeting. Nancy, France.
583 Kay, S. M., Ardolino, A. A., Gorring, M. L. and Ramos, V. A. 2007. The Somuncura Large
584 Igneous Province in Patagonia: interaction of a transient mantle thermal anomaly with a
585 subducting slab. Journal of Petrology 48(1): 43-77.
586 López, L., Jovic, S. M., Guido, D. M., Vidal, C. P., Páez, G. N. and Ruiz, R. 2015.
587 Geochemical
588 distribution and supergene behavior of indium at the Pingüino epithermal polymetallic vein
589 system, Patagonia, Argentina. Ore Geology Reviews 64:747-755.
590 Luna, G. L. 2021. Caracterización de los pulsos mineralizantes de la veta argentífera Julia
591 Norte, Proyecto Virginia, Macizo del Deseado, Santa Cruz, Argentina. Trabajo final de
592 licenciatura. Universidad Nacional del Sur. Inédito. 95 p. Bahía Blanca, Argentina.
593 Kay, S. M., Ardolino, A. A., Gorring, M. L. and Ramos, V. A. 2007. The Somuncura Large
594 Igneous Province in Patagonia: interaction of a transient mantle thermal anomaly with a
595 subducting slab. Journal of Petrology 48(1): 43-77.
596 Marfil, S.A., Maiza, P. and Pieroni, D. 2002. Mottramita-descloizita en un yacimiento de
597 caolín de la zona SE de Los Menucos (prov. de Río Negro). In VI Congreso de Mineralogía y
598 Metalogenia (Buenos Aires, 2002).

599 Maro, G. and Remesal, M.B. 2012. El volcanismo bimodal del colcán Cerro Corona, Alta
600 Sierra de SomúnCurá, provincia de Río Negro. Revista de la Asociación Geológica
601 Argentina 69(1): 142-151.
602 Martínez, H., Náñez, C., Lizuain, A., Dal Molin, C. N. and Turel, A.V. 2001. Hoja Geológica
603 4166-II San Antonio Oeste. Boletin Nº 254, Buenos Aires, 30 pp.
604 Mondillo, N., Herrington, R., Boyce, A. J., Wilkinson, C., Santoro, L. and Rumsey, M. 2018.
605 Critical elements in non-sulfide Zn deposits: a reanalysis of the Kabwe Zn-Pb ores (central
606 Zambia). Mineralogical Magazine 82(S1) : S89-S114.
607 Moura, M. A., Botelho, N. F. and de Mendonça, F. C. 2007. The indium-rich sulfides and rare
608 arsenates of the Sn–In-mineralized Mangabeira A-type granite, central Brazil. The Canadian
609 Mineralogist 45(3): 485-496.
610 Ogawa, Y., Ishiyama, D., Shikazono, N., Iwane, K., Kajiwara, M. and Tsuchiya, N. 2012. The
611 role of hydrous ferric oxide precipitation in the fractionation of arsenic, gallium, and indium
612 during the neutralization of acidic hot spring water by river water in the Tama River
613 watershed, Japan. Geochimica et Cosmochimica Acta 86:367-383.
614 Padelletti Di Marco, C. 2023. Estudio de las manifestaciones epitermales en dos sondajes
615 que interceptan las estructuras Del Indio y Griselda, Proyecto San Roque, Macizo
616 Norpatagónico, Argentina. Trabajo final de licenciatura. Universidad Nacional del Sur.
617 Inédito. 151 pp. Bahía Blanca, Argentina.
618 Padelletti Di Marco, C., Bouhier, V. and Ferracutti, G. 2023.Microtermometría de inclusiones
619 fluidas y análisis textural en esfalerita de las estructuras mineralizadas del Indio y Griselda,
620 Proyecto San Roque, Patagonia Argentina. XIV Congreso de Mineralogía, Petrología Ígnea y
621 Metamórfica.
622 Páez, G. N., Ruiz, R., Guido, D. M., Río, F. J., Subías, I., Recio, C. and Schalamuk, I. B.
623 2016.
624 High – grade ore shoots at the Martha epithermal vein system, Deseado Massif, Argentina:
625 The interplay of tectonic, hydrothermal and supergene processes in ore genesis. Ore
626 Geology

627 Reviews 72: 546-561.
628 Pankhurst, R. J., Riley, T. R., Fanning, C. M. and Kelley, S. P. 2000. Episodic silicic
629 volcanism in Patagonia and the Antarctic Peninsula: chronology of magmatism associated
630 with the break-
631 up of Gondwana. Journal of Petrology 41(5): 605-625.
632 Pavón Pivetta, C., Gregori, D., Benedini, L., Garrido, M., Strazzere, L., Geraldes, M., Costa
633 Dos Anderson, S. and Marcos, P. 2020. Contrasting tectonic settings in Northern Chon Aike
634 Igneous Province of Patagonia: Subduction and mantle plume-related volcanism in the Marifil
635 formation. International Geology Review 62(15): 1904-1930.
636 Permuy Vidal, C. 2014. Caracterización detallada de la mineralización en veta Eureka, y su
637 comparación con otras mineralizaciones del Distrito Cerro Negro, Macizo del Deseado,
638 Santa
639 Cruz, Argentina. Tesis Doctoral, Facultad de Ciencias Naturales y Museo de La Plata
640 (inedito),
641 273p. La Plata, Argentina.
642 Pavón Pivetta, C., Gregori, D., Benedini, L., Garrido, M., Strazzere, L., Geraldes, M., Costa
643 Dos Anderson, S. and Marcos, P. 2019. Contrasting tectonic settings in Northern Chon Aike
644 Igneous Province of Patagonia: Subduction and mantle plume-related volcanism in the Marifil
645 formation. International Geology Review 62(15): 1904-1930.
646 Plumlee, G.S. 1999. The environmental geology of mineral deposits. In: Plumlee, G.S.,
647 Logsdon, M.J. (Eds.), The Environmental Geochemistry of Mineral Deposits: Part A.
648 Processes, Methods, and Health Issues: Economic Geology 6A: 71-116.
649 Pugliese, F.E., Pugliese, L.E., Dahlquist, J.A., Basei, M.A.S. and Dopico, C.I.M. 2021.
650 Intermediate sulfidation epithermal Pb-Zn (±Ag±Cu±In) and low sulfidation Au (±Pb±Ag±Zn)
651 mineralization styles in the Gonzalito polymetallic mining district, North Patagonian Massif.
652 Journal of South American Earth Sciences 110: 103-388.
653 Reich, M. and Vasconcelos, P.M. 2015. Geological and economic significance of supergene
654 metal deposits. Elements 11(5): 305-310.

Reimann, C. and De Caritat, P. 2012. Chemical elements in the environment: factsheets for the geochemist and environmental scientist. Springer Science and Business Media.

Richmond, W.E. 1940. Crystal chemistry of the phosphates, arsenates, and vanadates of the type A/Oa(Z). American Mineralogist 25:441479.

Schalamuk, I., Zubia, M., Genini, A. and Fernandez, R. 1997. Jurassic epithermal Au-Ag deposits of Patagonia, Argentina. Ore Geology Reviews 12: 173-186.

Schwarz-Schampera, U. and Herzig, P. M. 2002. Indium: Geology, mineralogy, and economics. Springer Science & Business Media.

Schwellnus, C.M. 1945. Vanadium deposits in the Otavi Mountains, southwest Africa: South African Journal of Geology 48:49–73.

Scott, K.M. 1987. Solid solution in, and classification of, gossan-derived members of the alunite-jarosite family, northwest Queensland, Australia. American Mineralogist 72: 178-187.

Sillitoe, R., H. 2005. Supergene Oxidized and Enriched Porphyry Copper and Related Deposits, One Hundredth Anniversary Volume, Jeffrey W. Hedenquist, John F. H. Thompson, Richard J. Goldfarb, Jeremy P. Richards.

Sillitoe, R.H. 2019. Supergene oxidation of epithermal gold-silver mineralization in the Deseado massif, Patagonia, Argentina: Response to subduction of the Chile Ridge. Mineralium Deposita 54: 381-394.

Swedlund, P.J., Webster, J.G. and Miskelly, G.M. 2009. Goethite adsorption of Cu(II), Pb(II), Cd(II), and Zn(II) in the presence of sulfate: properties of the ternary complex. Geochimica et Cosmochimica Acta 73: 1548–1562.

Van der Westhuizen, W. A., Tordiffe, E. A. W., De Bruiyn, H. y Beukes, G. J. 1989. The composition of descloizite-mottramite in relation to the trace-element distribution of Pb, Zn, Cu and V in the Otavi Mountain Land, South West Africa/Namibia. Journal of Geochemical Exploration 34(1), 21-29.

Verhaert, M., Bernard, A., Dekoninck, A., Laorgue, L., Saddiqi, O. and Yans, J. 2017. Mineralogical and geochemical characterization of supergene Cu–Pb–Zn–V ores in the Oriental High Atlas, Morocco. Mineralium Deposita 52: 1049-1068.

683 Verhaert, M., Madi, A., El Basbas, A., Elharkaty, M., Oummouch, A., Oumohou, L., Yans, J.
684 2020. Genesis of As-Pb-Rich Supergene Mineralization: The Tazalaght and Agoujgal Cu
685 Deposits (Moroccan Anti-Atlas Copperbelt). Economic Geology 115(8): 1725-1748.
686 Verwoerd, W.J. 1953. The mineralogy and genesis of the lead-zinc-vanadium deposit of
687 Abenab West in the Otavi Mountains, South West Africa. Doctoral dissertation, Stellenbosch,
688 Stellenbosch University, 328 p.
689 Vlasáč, J., Mikuš, T., Ondrejka, M., Žitňan, P. and Tuček, P. 2021. Supergene Pb-Cu-(Sb)
690 mineral assemblage in abandoned epithermal deposit Rudno nad Hronom, Slovakia. Ageos,
691 13(1):107-118.
692 Wood, S. A. and Samson, I. M. 2006. The aqueous geochemistry of gallium, germanium,
693 indium and scandium. Ore Geology Reviews 28(1): 57-102.
694 Wright, M.T. and Belitz, K. 2010. Factors controlling the regional distribution of Vanadium in
695 groundwater. Ground Water 48: 515-525.
696 Yans, J., Verhaert, M., Dekoninck, A., Bernard, A., Gautheron, C. and Saddiqi, O. 2017.
697 Genesis of the mottramite-bearing Jbel Haouanit Cu–Pb–Zn–V supergene ore deposit
698 (Eastern High Atlas, Morocco). In Proceedings of the 14th SGA Biennial Meeting, 20-23
699 August 2017, Québec City, Canada pp. 1599-1602.
700 Zappettini, E., O. 2021. Minerales y Metales Críticos y Estratégicos. Análisis de Situación y
701 Metodología de Clasificación para la República Argentina. Serie Contribuciones Técnicas
702 Recursos Minerales N°45, 19 p. Buenos Aires, Servicio Geológico Minero Argentino. Instituto
703 de Geología y Recursos Minerales.
704

FIGURE CAPTIONS

Figure 1: a) Geological map of the northeast sector of the Northpatagonian Massif and location of the San Roque project. Modified from Martínez et al. (2001). **b)** Geological map of San Roque project in Del Indio and Griselda structures area. Modified from Falls and Montgomery (2012).

Figure 2: a-b) Columnar lithological profiles of the analyzed drillholes. **c)** Hand sample of the polymictic orthobreccia subfacies extracted from the hypogene zone, MF-DDH-04 drillhole. **d)** Hand sample of the polymictic orthobreccia subfacies extracted from the supergene zone, MF-DDH-02 drillhole. **e)** Hand sample of the mudstone subfacies extracted from the supergene zone, MF-DDH-02 drillhole. **f)** Hand sample from a hydrothermal breccia located in the zone of supergene alteration, MF-DDH-04 drillhole. **g)** Hand sample from a quartz and oxidized sulfides vein located in the zone of supergene alteration, MF-DDH-02 drillhole. Qz: quartz, Hem: hematite, Mn- Fe Ox-Hx: Mn-Fe oxy-hydroxides, Mott: mottramite, Py: pyrite, Cor: coronadite, Fcor: ferricoronadite; Pjrs: plumbojarosite. Flr: fluorite.

Figure 3: Boxplots showing the chemical variation in studied drillholes.

Figure 4: Lithogeochemical profiles corresponding to **a)** MF-DDH-02 and **b)** MF-DDH-04 studied drillholes.

Figure 5: a) Quartz and sulphide veins with intense oxidation hosted in the polymictic orthobreccia subfacies. The yellow arrows indicate dissolution cavities. **b)** Photomicrograph of subhedral pyrite crystals partially replaced by hematite. **c)** Photomicrographs of hematite crystals with pyrite core and late mottramite crystals. **d)** Quartz hydrothermal vein with dissolution voids and open spaces partially filled by supergene minerals. **e)** Late colloform coronadite aggregates. **f)** Backscattered electron image of coronadite in secondary electrons mode. **g)** Late prismatic crystals of mottramite that grow on late cavities and within hematite. **h)** Microfractures filled by late mottramite. **i)** Colloform aggregate of mottramite. **j)** Plumbojarosite fine-grained aggregate in the polymictic orthobreccia. **k-m)** Plumbojarosite

and hematite crystals under the transmitted light microscope. Qz: quartz, Hem: hematite, Mn-Fe Ox-Hx: Mn-Fe oxy-hydroxides, Mott: mottramite, Py: pyrite, Cor: coronadite, Fcor: ferricoronadite, Pjrs: plumbojarosite, Gp: gypsum.

Figure 6: Backscattered electron images with distribution of chemical element concentrations (chemical maps) of hematite and mottramite. Yellow circles indicate the semiquantitative analyses position (Appendix B, Table 3).

Figure 7: Backscattered electron images with distribution of chemical element concentrations (chemical maps) of plumbojarosite.

Figure 8: Graph showing the variations in the vanadium content ranges in the lithologies present in the San Roque project and in Northpatagonian massif region. Fm.: Formation. The references of the geological units are ordered according to the distance from the area of the San Roque project, as follows: 1: Asiain et al. (2019); 2: Asiain et al. (2021); 3: Ferracutti et al. (2022); 4: Asiain et al. (2017, 2019); 5: Pavón Pivetta et al. (2020); 6: Maro y Remesal (2012); 7: Pugliese et al. (2021); 8: Asiain et al. (2017); 9 y 10: Marifil S.A. (private report).

Figure 8: Graph showing the the vanadium content ranges in the lithologies present in the San Roque project and in Northpatagonian massif region. The references of the geological units are ordered according to the distance from the area of the San Roque project, as follows: 1: Asiain et al. (2019); 2: Asiain et al. (2021); 3: Ferracutti et al. (2022); 4: Asiain et al. (2017, 2019); 5: Pavón Pivetta et al. (2020); 6: Maro y Remesal (2012); 7: Pugliese et al. (2021); 8: Asiain et al. (2017); 9 y 10: Marifil S.A. (private report).

Figura 1

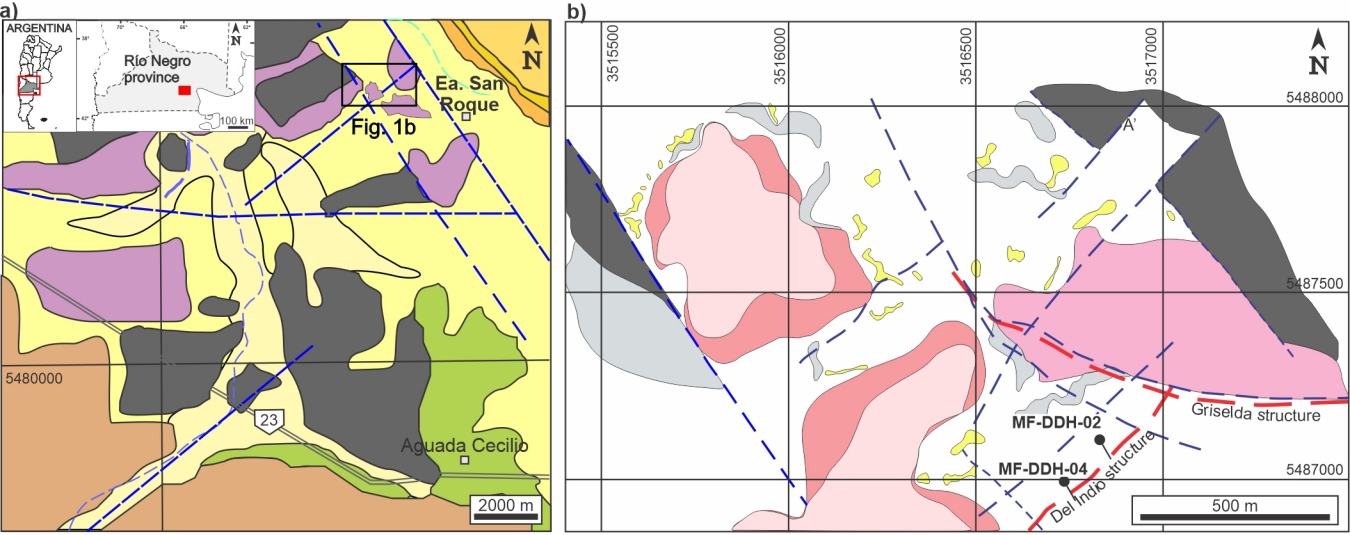

LEGEND

- Alluvial deposits - (*Holocene*)
- Colluvial deposits - (*Holocene*)
- "*Rodados Patagónicos*" - (*Pliocene - Pleistocene*)
- Río Negro Formation - (*Pliocene*)
- Gran Bajo del Gualicho Formation - (*Oligocene - Miocene*)
- Somuncurá Formation - (*Oligocene - Miocene*)
- Arroyo Barbudo Formation - (*Cretaceous - Paleocene*)
- Marifil Volcanic Complex - (*Early Jurassic*)
- Nahuel Niyeu Formation - (*Early Cambrian*)

LEGEND

- Aluvial and colluvial deposits
- Rhyolitic porphyry
- Quartz trachyte
- Rhyolitic tuff
- Ignimbrite
- Epiclastic facies

Marifil Volcanic Complex - (*Early Jurassic*)

- Nahuel Niyeu Formation - (*Early Cambrian*)
- Studied drillhole
- Mineralized structure
- Fault

Figure 2

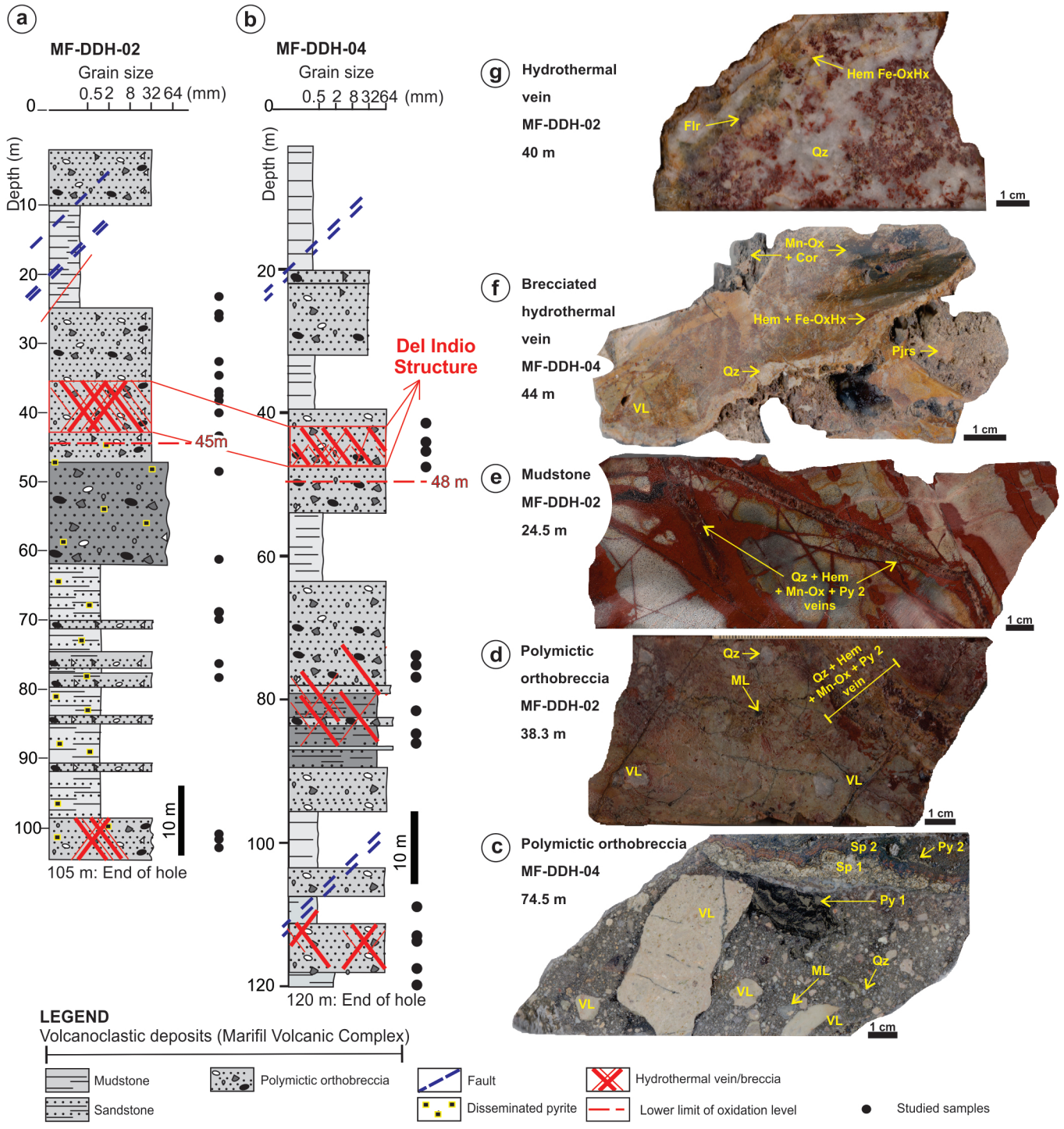
a
MF-DDH-02
Grain size
0.5 2 8 32 64 (mm)
0
Depth (m)
10
20
30
40
45m
50
60
70
80
90
100
10 m
105 m: End of hole
b
MF-DDH-04
Grain size
0.5 2 8 32 64 (mm)
0
Depth (m)
20
40
48 m
60
80
100
10 m
120
120 m: End of hole
Del Indio Structure
g
Hydrothermal vein
MF-DDH-02
40 m
Hem Fe-OxHx
Flr
Qz
1 cm
f
Brecciated hydrothermal vein
MF-DDH-04
44 m
Mn-Ox + Cor
Hem + Fe-OxHx
Pjrs
Qz
VL
1 cm
e
Mudstone
MF-DDH-02
24.5 m
Qz + Hem + Mn-Ox + Py 2 veins
1 cm
d
Polymictic orthobreccia
MF-DDH-02
38.3 m
Qz
ML
Qz + Hem + Mn-Ox + Py 2 vein
VL
VL
1 cm
c
Polymictic orthobreccia
MF-DDH-04
74.5 m
Sp 2
Py 2
Sp 1
Py 1
VL
ML
Qz
VL
VL
VL
1 cm
LEGEND
Volcanoclastic deposits (Marifil Volcanic Complex)
Mudstone
Sandstone
Polymictic orthobreccia
Fault
Disseminated pyrite
Hydrothermal vein/breccia
Lower limit of oxidation level
Studied samples

Figure 3

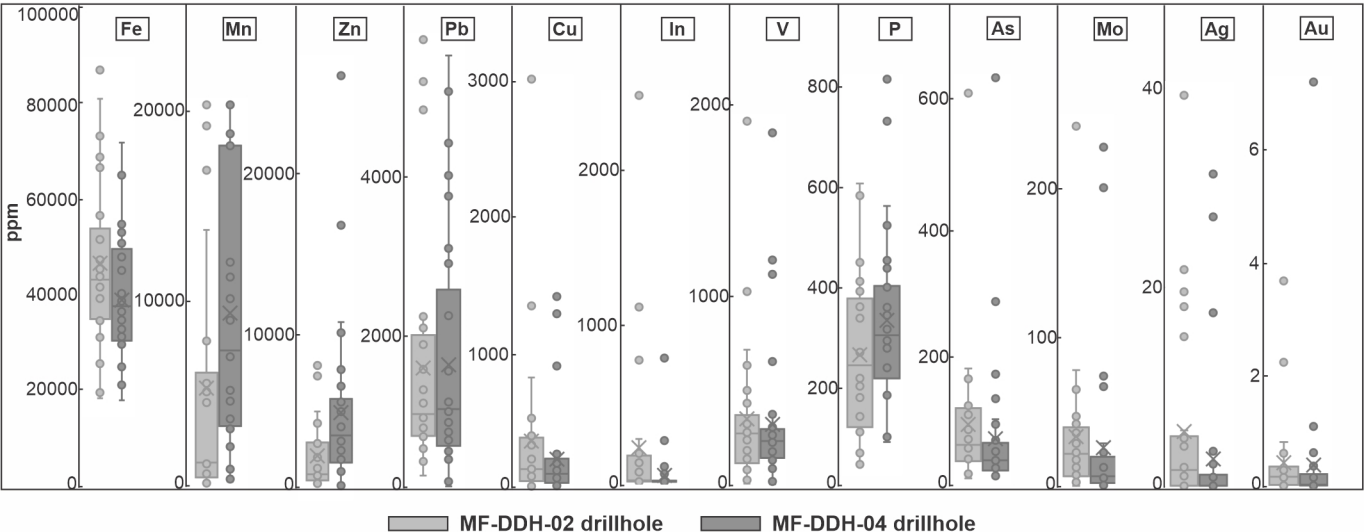
ppm
Fe
Mn
Zn
Pb
Cu
In
V
P
As
Mo
Ag
Au
MF-DDH-02 drillhole
MF-DDH-04 drillhole

Figure 4

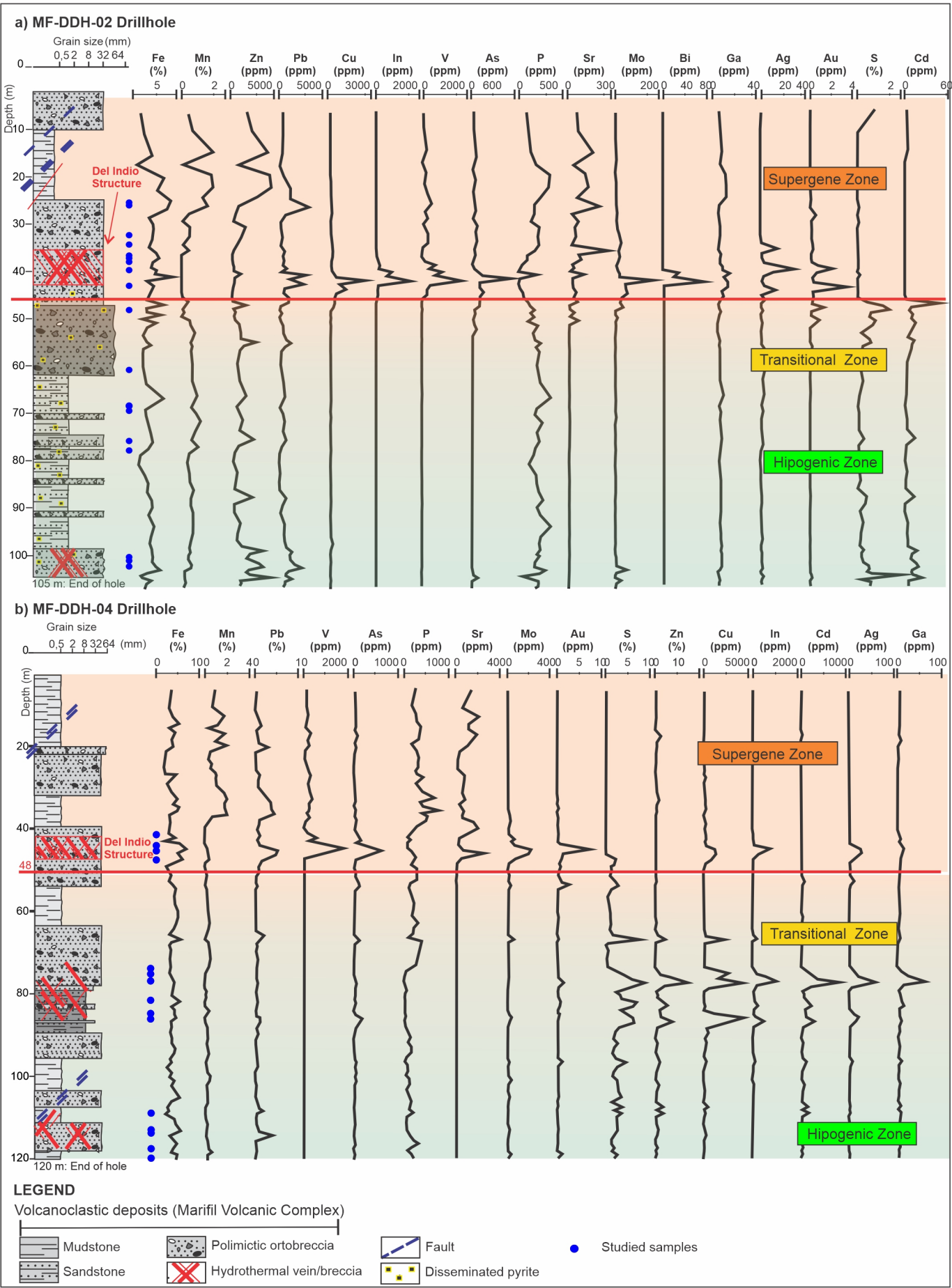
a) MF-DDH-02 Drillhole
Grain size (mm)
0,5 2 8 32 64
Fe (%)
Mn (%)
Zn (ppm)
Pb (ppm)
Cu (ppm)
In (ppm)
V (ppm)
As (ppm)
P (ppm)
Sr (ppm)
Mo (ppm)
Bi (ppm)
Ga (ppm)
Ag (ppm)
Au (ppm)
S (%)
Cd (ppm)
Depth (m)
Del Indio Structure
Supergene Zone
Transitional Zone
Hipogenic Zone
105 m: End of hole
b) MF-DDH-04 Drillhole
Grain size
0,5 2 8 32 64 (mm)
Fe (%)
Mn (%)
Pb (%)
V (ppm)
As (ppm)
P (ppm)
Sr (ppm)
Mo (ppm)
Au (ppm)
S (%)
Zn (%)
Cu (ppm)
In (ppm)
Cd (ppm)
Ag (ppm)
Ga (ppm)
Depth (m)
Del Indio Structure
48
Supergene Zone
Transitional Zone
Hipogenic Zone
120 m: End of hole
LEGEND
Volcanoclastic deposits (Marifil Volcanic Complex)
Mudstone
Sandstone
Polimictic ortobreccia
Hydrothermal vein/breccia
Fault
Disseminated pyrite
Studied samples

Figura 5

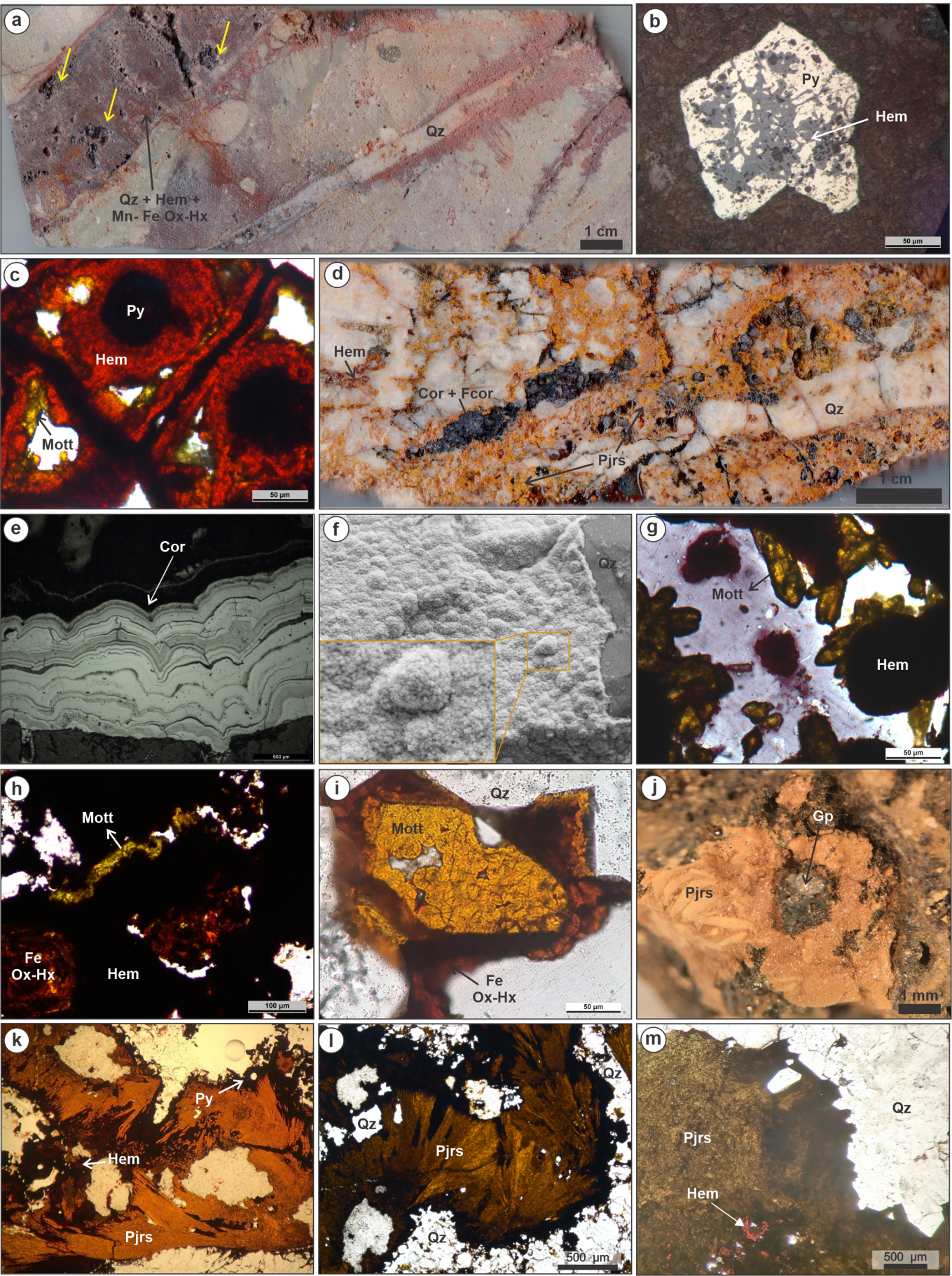
a
Qz
Qz + Hem +
Mn- Fe Ox-Hx
1 cm
b
Py
Hem
50 µm
c
Py
Hem
Mott
50 µm
d
Hem
Cor + Fcor
Qz
Pjrs
1 cm
e
Cor
500 µm
f
Qz
g
Mott
Hem
50 µm
h
Mott
Fe
Ox-Hx
Hem
100 µm
i
Qz
Mott
Fe
Ox-Hx
50 µm
j
Gp
Pjrs
1 mm
k
Py
Hem
Pjrs
l
Qz
Qz
Pjrs
Qz
500 µm
m
Qz
Pjrs
Hem
500 µm

Figura 6

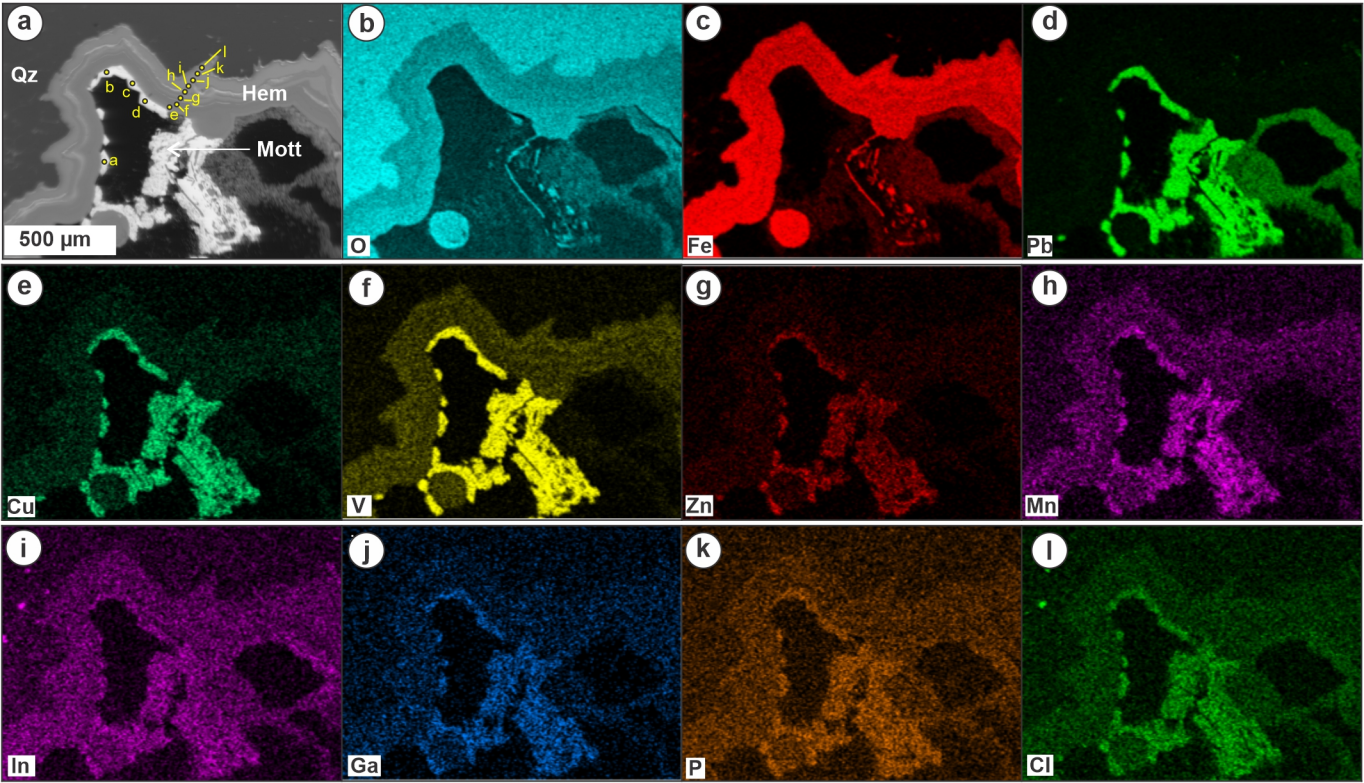

Figura 7

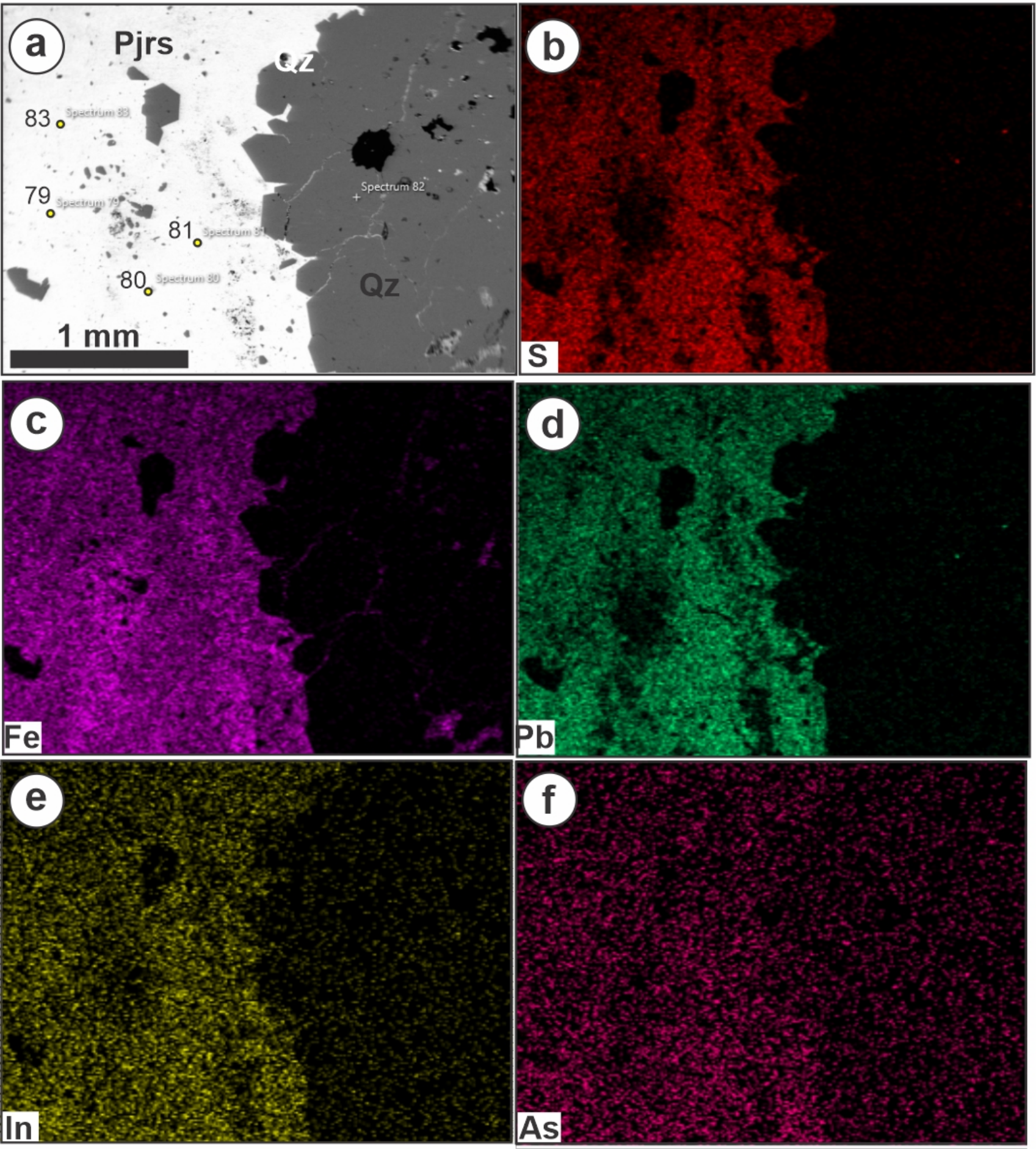
a
Pjrs
Qz
83
Spectrum 83
79
Spectrum 79
81
Spectrum 81
80
Spectrum 80
Spectrum 82
Qz
1 mm
b
S
c
Fe
d
Pb
e
In
f
As

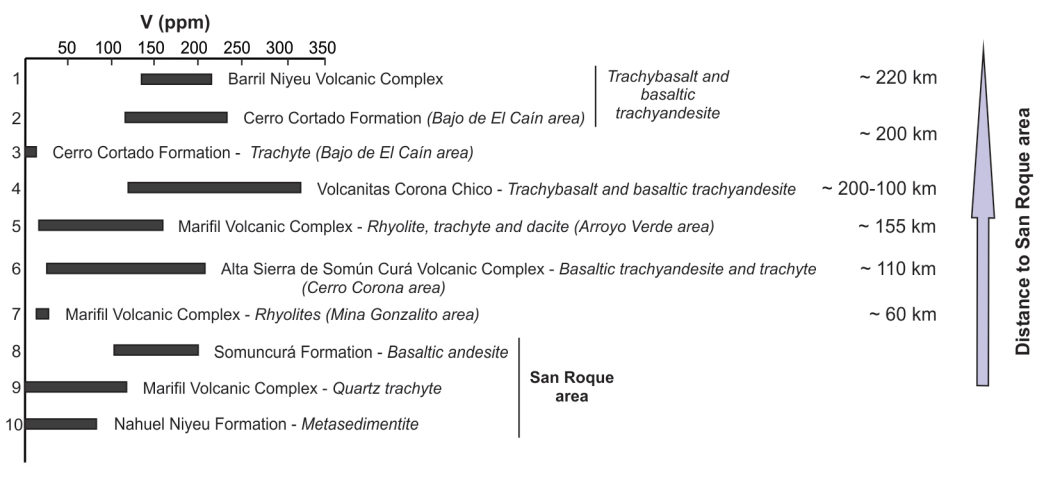
V (ppm)
50 100 150 200 250 300 350
1 Barril Niyeu Volcanic Complex
2 Cerro Cortado Formation (Bajo de El Caín area)
3 Cerro Cortado Formation - Trachyte (Bajo de El Caín area)
4 Volcanitas Corona Chico - Trachybasalt and basaltic trachyandesite
5 Marifil Volcanic Complex - Rhyolite, trachyte and dacite (Arroyo Verde area)
6 Alta Sierra de Somún Curá Volcanic Complex - Basaltic trachyandesite and trachyte (Cerro Corona area)
7 Marifil Volcanic Complex - Rhyolites (Mina Gonzalito area)
8 Somuncurá Formation - Basaltic andesite
9 Marifil Volcanic Complex - Quartz trachyte
10 Nahuel Niyeu Formation - Metasedimentite
Trachybasalt and basaltic trachyandesite
San Roque area
~ 220 km
~ 200 km
~ 200-100 km
~ 155 km
~ 110 km
~ 60 km
Distance to San Roque area

Appendix A. Pearson correlation coefficients calculated with the geochemical data of all the samples located in the oxidation zone of the MF-DDH-04 drillhole

	In	Au	Ag	As	Cd	Co	Cr	Cu	Fe	Ga	Mn	Mo	Ni	P	Pb	S	V	Zn	Zr	Al	Ba	Ca	K	La	Li	Mg	Na	Sr	Y
In	1,00																												
Au	0,97	1,00																											
Ag	0,78	0,73	1,00																										
As	0,97	0,93	0,79	1,00																									
Cd	-0,04	0,00	0,03	0,07	1,00																								
Co	-0,32	-0,28	-0,29	-0,32	0,44	1,00																							
Cr	-0,01	-0,02	0,07	0,03	0,41	0,60	1,00																						
Cu	0,77	0,73	0,98	0,80	0,03	-0,31	-0,04	1,00																					
Fe	0,49	0,53	0,54	0,57	0,24	0,16	0,16	0,62	1,00																				
Ga	0,65	0,61	0,69	0,69	0,11	-0,15	0,55	0,61	0,46	1,00																			
Mn	-0,29	-0,27	-0,33	-0,29	0,32	0,75	0,05	-0,27	0,15	-0,51	1,00																		
Mo	0,88	0,81	0,93	0,92	-0,05	-0,41	-0,02	0,93	0,57	0,69	-0,36	1,00																	
Ni	-0,30	-0,26	-0,29	-0,30	0,40	0,91	0,83	-0,35	0,09	0,08	0,49	-0,39	1,00																
P	-0,37	-0,32	-0,34	-0,40	-0,03	0,47	-0,06	-0,29	-0,02	-0,57	0,53	-0,38	0,34	1,00															
Pb	0,54	0,51	0,55	0,53	-0,04	0,09	-0,19	0,62	0,62	0,13	0,39	0,57	-0,13	0,20	1,00														
S	0,03	0,16	0,38	0,05	0,24	-0,05	0,07	0,36	0,31	0,32	-0,26	0,15	-0,04	-0,15	0,01	1,00													
V	0,88	0,79	0,71	0,91	-0,02	-0,33	-0,04	0,74	0,59	0,59	-0,19	0,88	-0,33	-0,36	0,56	-0,11	1,00												
Zn	-0,21	-0,19	-0,25	-0,15	0,74	0,66	0,27	-0,20	0,17	-0,28	0,75	-0,27	0,53	0,43	0,17	-0,16	-0,10	1,00											
Zr	-0,36	-0,33	-0,17	-0,33	0,65	0,73	0,62	-0,22	0,04	0,01	0,48	-0,36	0,73	0,26	-0,09	0,26	-0,36	0,66	1,00										
Al	-0,22	-0,21	-0,04	-0,17	0,45	0,68	0,87	-0,12	0,14	0,36	0,23	-0,20	0,82	0,03	-0,14	0,16	-0,27	0,36	0,78	1,00									
Ba	-0,36	-0,35	-0,39	-0,34	0,29	0,74	0,28	-0,39	-0,04	-0,36	0,72	-0,42	0,58	0,47	0,01	-0,23	-0,28	0,60	0,55	0,41	1,00								
Ca	0,05	0,01	0,16	0,15	0,91	0,46	0,48	0,14	0,24	0,16	0,33	0,10	0,43	0,05	0,10	0,03	0,13	0,74	0,63	0,47	0,29	1,00							
K	-0,39	-0,38	-0,08	-0,36	0,07	0,43	0,42	-0,12	-0,01	0,03	0,12	-0,25	0,44	0,29	-0,08	0,34	-0,39	0,04	0,58	0,60	0,41	0,12	1,00						
La	-0,69	-0,66	-0,65	-0,72	-0,03	0,32	0,33	-0,72	-0,50	-0,28	0,02	-0,72	0,47	0,20	-0,74	-0,13	-0,71	0,02	0,34	0,41	0,31	-0,08	0,41	1,00					
Li	-0,27	-0,25	-0,24	-0,23	0,51	0,85	0,75	-0,29	0,16	0,12	0,52	-0,32	0,90	0,28	0,00	-0,06	-0,29	0,59	0,73	0,85	0,52	0,52	0,37	0,32	1,00				
Mg	-0,18	-0,18	-0,20	-0,13	0,67	0,67	0,84	-0,28	0,02	0,27	0,27	-0,26	0,82	-0,03	-0,31	-0,10	-0,19	0,56	0,72	0,85	0,43	0,66	0,28	0,43	0,85	1,00			
Na	0,22	0,24	0,15	0,22	0,16	0,43	0,24	0,18	0,43	0,11	0,29	0,15	0,32	0,23	0,34	0,07	0,23	0,22	0,19	0,22	0,22	0,25	0,32	-0,20	0,25	0,16	1,00		
Sr	0,08	0,00	0,27	0,16	0,33	0,26	0,40	0,25	0,19	0,21	0,13	0,22	0,25	0,03	0,15	-0,20	0,12	0,27	0,32	0,50	0,30	0,51	0,37	0,05	0,38	0,46	0,20	1,00	
Y	-0,41	-0,37	-0,43	-0,41	0,55	0,84	0,55	-0,45	-0,11	-0,26	0,57	-0,52	0,82	0,41	-0,22	-0,15	-0,40	0,71	0,74	0,58	0,62	0,58	0,30	0,47	0,72	0,72	0,32	0,20	1,00

0.1 - 0.4	Low
0.41 - 0.7	Moderate
0.71 - 0.9	High
0.91 - 1	Perfect

Tabla 1 - Semi-quantitative chemical analyzes in hematite

	Element	O	Al	Si	S	Cl	K	Ca	V	Mn	Fe	In	Cu	Zn	As	Mo	Total:
	Analysis	Wt%															
DHH-02; 40.6m	S67	38.97	3.18	1.51	b.d.l	b.d.l	0.27	0.47	1.14	b.d.l	50.26	b.d.l	2.55	b.d.l	1.64	b.d.l	100
	S69	38.62	b.d.l	1.49	b.d.l	b.d.l	b.d.l	b.d.l	0.53	58.59	b.d.l	b.d.l	b.d.l	b.d.l	b.d.l	0.77	100
	S70	30.74	1.94	2.51	b.d.l	b.d.l	0.25	0.37	01.02	0.59	60.16	b.d.l	1.22	b.d.l	0.57	0.63	100
	S68	38.91	3.15	1.43	b.d.l	b.d.l	0.29	0.5	1.28	b.d.l	50.16	b.d.l	2.51	b.d.l	1.78	b.d.l	100
	S60	45.25	3.96	10.11	0.41	1.22	0.67	b.d.l	1.85	b.d.l	35.47	b.d.l	0.82	0.24	b.d.l	b.d.l	100
	S64	40.12	02.06	2.25	b.d.l	b.d.l	b.d.l	b.d.l	1.63	b.d.l	53.5	b.d.l	b.d.l	b.d.l	b.d.l	0.44	100
	S65	40.04	2.55	2.12	0.26	b.d.l	b.d.l	b.d.l	1.64	b.d.l	53.39	b.d.l	b.d.l	b.d.l	b.d.l	b.d.l	100
	S66	43.91	2.65	1.98	b.d.l	b.d.l	b.d.l	b.d.l	01.05	b.d.l	50.41	b.d.l	b.d.l	b.d.l	b.d.l	b.d.l	100
DDH-04-44.5m	a	40.99	b.d.l	0.85	0.19	b.d.l	b.d.l	0.35	1.77	b.d.l	55.84	b.d.l	b.d.l	b.d.l	b.d.l	b.d.l	100
	b	41.12	b.d.l	0.82	0.2	b.d.l	b.d.l	0.29	1.77	b.d.l	55.8	b.d.l	b.d.l	b.d.l	b.d.l	b.d.l	100
	c	41.43	b.d.l	0.78	0.23	b.d.l	b.d.l	0.3	1.67	b.d.l	55.59	b.d.l	b.d.l	b.d.l	b.d.l	b.d.l	100
	d	45.84	3.58	0.71	0.26	b.d.l	b.d.l	0.71	1.83	0.15	46.91	b.d.l	b.d.l	b.d.l	b.d.l	b.d.l	100
	e	47.13	2.9	1.26	b.d.l	b.d.l	b.d.l	0.5	1.8	b.d.l	46.41	b.d.l	b.d.l	b.d.l	b.d.l	b.d.l	100
	f	45.87	03.03	0.71	0.31	b.d.l	b.d.l	0.69	1.94	b.d.l	47.44	b.d.l	b.d.l	b.d.l	b.d.l	b.d.l	100
	g	45.1	2.56	0.57	b.d.l	b.d.l	b.d.l	0.51	1.8	b.d.l	48.14	1.33	b.d.l	b.d.l	b.d.l	b.d.l	100
	h	44.98	2.63	0.57	0.28	b.d.l	b.d.l	0.54	1.8	b.d.l	47.91	1.3	b.d.l	b.d.l	b.d.l	b.d.l	100
	i	39.97	1.66	0.63	0.34	b.d.l	b.d.l	0.42	2.42	0.87	52.73	0.98	b.d.l	b.d.l	b.d.l	b.d.l	100
	j	43.15	1.31	0.56	0.31	b.d.l	b.d.l	0.35	2.5	0.84	50.17	0.82	b.d.l	b.d.l	b.d.l	b.d.l	100
	k	44.01	2.26	0.63	0.32	b.d.l	b.d.l	0.45	1.98	0.57	48.48	1.3	b.d.l	b.d.l	b.d.l	b.d.l	100
	l	42	1.36	0.59	0.34	b.d.l	b.d.l	0.35	2.52	0.79	51.24	0.81	b.d.l	b.d.l	b.d.l	b.d.l	100

	Element	O	Al	Si	S	Cl	K	Ca	V	Mn	Fe	In	Cu	Zn	As	Mo	Total:
	Analysis	Atomic %															
DHH-02; 40.6m	S67	67,47	3,26	1,49	b.d.l	b.d.l	0,19	0,33	0,62	b.d.l	24,93	b.d.l	1,11	b.d.l	0,61	b.d.l	100
	S69	68,3	b.d.l	1,5	b.d.l	b.d.l	b.d.l	b.d.l	0,29	b.d.l	29,68	b.d.l	b.d.l	b.d.l	b.d.l	0,23	100
	S70	59,31	2,21	2,75	b.d.l	b.d.l	0,2	0,29	0,62	0,33	33,25	b.d.l	0,59	b.d.l	0,23	0,2	100
	S68	67,44	3,24	1,41	b.d.l	b.d.l	0,2	0,34	0,7	b.d.l	24,91	b.d.l	1,09	b.d.l	0,66	b.d.l	100
	S60	69,2	3,59	8,81	0,31	0,84	0,42	b.d.l	0,89	b.d.l	15,54	b.d.l	0,32	0,09	b.d.l	b.d.l	100
	S64	68,54	2,08	2,19	b.d.l	b.d.l	b.d.l	b.d.l	0,87	b.d.l	26,18	b.d.l	b.d.l	b.d.l	b.d.l	0,13	100
	S65	68,21	2,57	2,06	0,22	b.d.l	b.d.l	b.d.l	0,88	b.d.l	26,06	b.d.l	b.d.l	b.d.l	b.d.l	b.d.l	100
	S66	71,54	2,56	1,84	b.d.l	b.d.l	b.d.l	b.d.l	0,53	b.d.l	23,53	b.d.l	b.d.l	b.d.l	b.d.l	b.d.l	100
DDH-04-44.5m	a	70,35	b.d.l	0,84	0,17	b.d.l	b.d.l	0,24	0,96	b.d.l	27,45	b.d.l	b.d.l	b.d.l	b.d.l	b.d.l	100
	b	70,48	b.d.l	0,8	0,17	b.d.l	b.d.l	0,2	0,95	b.d.l	27,4	b.d.l	b.d.l	b.d.l	b.d.l	b.d.l	100
	c	70,75	b.d.l	0,76	0,2	b.d.l	b.d.l	0,21	0,89	b.d.l	27,19	b.d.l	b.d.l	b.d.l	b.d.l	b.d.l	100
	d	72,94	3,38	0,65	0,21	b.d.l	b.d.l	0,45	0,91	0,07	21,39	b.d.l	b.d.l	b.d.l	b.d.l	b.d.l	100
	e	74,07	2,7	1,13	b.d.l	b.d.l	b.d.l	0,32	0,89	b.d.l	20,9	b.d.l	b.d.l	b.d.l	b.d.l	b.d.l	100
	f	73,16	2,86	0,65	0,24	b.d.l	b.d.l	0,44	0,97	b.d.l	21,68	b.d.l	b.d.l	b.d.l	b.d.l	b.d.l	100
	g	73,12	2,46	0,53	b.d.l	b.d.l	b.d.l	0,33	0,92	b.d.l	22,36	0,3	b.d.l	b.d.l	b.d.l	b.d.l	100
	h	72,91	2,52	0,53	0,23	b.d.l	b.d.l	0,35	0,92	b.d.l	22,25	0,29	b.d.l	b.d.l	b.d.l	b.d.l	100
	i	69,03	1,7	0,62	0,29	b.d.l	b.d.l	0,29	1,31	0,44	26,09	0,23	b.d.l	b.d.l	b.d.l	b.d.l	100
	j	71,85	1,29	0,53	0,26	b.d.l	b.d.l	0,23	1,31	0,41	23,93	0,19	b.d.l	b.d.l	b.d.l	b.d.l	100
	k	72,26	2,2	0,59	0,27	b.d.l	b.d.l	0,29	1,02	0,27	22,8	0,3	b.d.l	b.d.l	b.d.l	b.d.l	100
	l	70,87	1,36	0,57	0,28	b.d.l	b.d.l	0,24	1,34	0,39	24,77	0,19	b.d.l	b.d.l	b.d.l	b.d.l	100

Tabla 2 - Semi-quantitative chemical analyzes in manganese oxides

	Element	O	Al	Si	Ca	V	Mn	Fe	Cu	Zn	As	Pb	Total:
	Analysis	Wt%											
DDH-04; 4-3	S4	14,13	0,52	0,39	b.d.l.	2,06	51,35	6,7	1,5	b.d.l.	b.d.l.	23,34	100
	S5	31,87	0,84	0,17	b.d.l.	1,54	36,28	b.d.l.	0,92	0,47	b.d.l.	27,91	100
	S6	31,84	0,76	b.d.l.	b.d.l.	1,55	36,93	b.d.l.	1,11	b.d.l.	b.d.l.	27,81	100
	S9	35,08	0,86	b.d.l.	b.d.l.	1,44	34,17	b.d.l.	0,94	b.d.l.	b.d.l.	27,51	100
	S10	30,1	0,69	0,37	b.d.l.	1,63	37,54	b.d.l.	1,14	b.d.l.	b.d.l.	28,52	100
	S11	15,7	0,48	0,39	b.d.l.	2,05	55,94	b.d.l.	1,43	b.d.l.	b.d.l.	24,01	100
	S12	31,26	0,86	b.d.l.	b.d.l.	1,51	36,93	b.d.l.	1,15	b.d.l.	b.d.l.	28,29	100
	S15	36,34	0,87	0,25	b.d.l.	1,38	33,08	b.d.l.	0,97	b.d.l.	b.d.l.	27,11	100
	S16	29,71	0,85	b.d.l.	b.d.l.	1,55	38,07	b.d.l.	1,28	b.d.l.	b.d.l.	28,54	100
	S17	30,75	0,79	b.d.l.	b.d.l.	1,58	37,43	b.d.l.	1,36	b.d.l.	b.d.l.	28,09	100
	S27	25,94	0,66	0,27	0,48	1,65	36,76	11,13	2,58	b.d.l.	1,47	19,07	100
	S28	29,56	0,61	3,46	0,47	1,45	33,47	10,5	1,82	b.d.l.	1,82	16,84	100
	S29	35,01	0,76	0,32	0,52	1,37	30,41	8,69	1,51	b.d.l.	1,38	20,05	100

	Element	O	Al	Si	Ca	V	Mn	Fe	Cu	Zn	As	Pb	Total:
	Analysis	Atomic %											
DDH-04; 4-3	S4	41,12	0,9	0,65	b.d.l.	1,89	43,51	5,59	1,1	b.d.l.	b.d.l.	5,24	100
	S5	69,26	1,08	0,21	b.d.l.	1,05	22,96	b.d.l.	0,5	0,25	b.d.l.	4,68	100
	S6	69,28	0,98	b.d.l.	b.d.l.	1,06	23,4	b.d.l.	0,61	b.d.l.	b.d.l.	4,67	100
	S9	72,55	1,05	b.d.l.	b.d.l.	0,93	20,58	b.d.l.	0,49	b.d.l.	b.d.l.	4,39	100
	S10	67,41	0,91	0,47	b.d.l.	1,14	24,48	b.d.l.	0,64	b.d.l.	b.d.l.	4,93	100
	S11	44,41	0,8	0,63	b.d.l.	1,82	46,08	b.d.l.	1,01	b.d.l.	b.d.l.	5,24	100
	S12	68,75	1,12	b.d.l.	b.d.l.	1,04	23,65	b.d.l.	0,63	b.d.l.	b.d.l.	4,8	100
	S15	73,56	1,04	0,29	b.d.l.	0,88	19,5	b.d.l.	0,49	b.d.l.	b.d.l.	4,24	100
	S16	67,05	1,14	b.d.l.	b.d.l.	1,1	25,02	b.d.l.	0,73	b.d.l.	b.d.l.	4,97	100
	S17	68,14	1,04	b.d.l.	b.d.l.	1,1	24,16	b.d.l.	0,76	b.d.l.	b.d.l.	4,81	100
	S27	59,54	0,9	0,35	0,44	1,19	24,57	7,32	1,49	0,83	b.d.l.	3,38	100
	S28	62,24	0,77	4,15	0,39	0,96	20,52	6,33	0,96	0,94	b.d.l.	2,74	100
	S29	70,17	0,91	0,36	0,42	0,86	17,75	4,99	0,76	0,68	b.d.l.	3,1	100

Table 3 - Semi-quantitative chemical analyzes in mottramite

	Element	O	V	Mn	Fe	Cu	Zn	Pb	Al	Si	Total:
	Analysis	Wt%									
DHH-02; 40.6m	S55	19,73	11,58	b.d.l.	0,71	12,27	b.d.l.	55,71	b.d.l	b.d.l	100
	S56	20,56	11,65	b.d.l.	b.d.l.	11,9	b.d.l.	55,38	0,5	b.d.l	100
	S57	18,93	11,74	b.d.l.	0,6	12,66	b.d.l.	56,07	b.d.l	b.d.l	100
	S58	18,38	11,78	b.d.l.	b.d.l.	12,81	b.d.l.	57,03	b.d.l	b.d.l	100
	S59	20,04	11,82	b.d.l.	0,71	12,88	b.d.l.	54,54	b.d.l	b.d.l	100
	S61	21,08	10,21	b.d.l.	10,22	11,27	b.d.l.	47,23	b.d.l	b.d.l	100
	S62	18,06	11,73	b.d.l.	0,53	12,56	b.d.l.	57,12	b.d.l	b.d.l	100
	S63	19,13	11,59	b.d.l.	0,42	13,02	b.d.l.	54,27	0,89	0,68	100
DDH-04-44.5m	a	18,77	11,75	0,75	b.d.l.	7,93	3,6	56,55	b.d.l.	b.d.l.	100
	b	18,06	11,99	1	0,65	8,03	3,6	57,32	b.d.l.	b.d.l.	100
	c	18,35	12,04	1,02	b.d.l.	11,1	b.d.l.	57,49	b.d.l.	b.d.l.	100
	d	17,86	12,14	0,6	b.d.l.	6,7	5,57	57,12	b.d.l.	b.d.l.	100

	Element	O	V	Mn	Fe	Cu	Zn	Pb	Al	Si	Total:
	Analysis	Atomic %									
DHH-02; 40.6m	S55	63,73	11,75	b.d.l.	0,66	9,97	b.d.l.	13,89	b.d.l.	b.d.l.	100
	S56	64,68	11,51	b.d.l.	b.d.l.	9,43	b.d.l.	13,45	0,93	b.d.l.	100
	S57	62,46	12,16	b.d.l.	0,56	10,52	b.d.l.	14,29	b.d.l.	b.d.l.	100
	S58	61,87	12,45	b.d.l.	b.d.l.	10,85	b.d.l.	14,82	b.d.l.	b.d.l.	100
	S59	63,8	11,81	b.d.l.	0,65	10,33	b.d.l.	13,41	b.d.l.	b.d.l.	100
	S61	62,55	9,52	b.d.l.	8,69	8,42	b.d.l.	10,82	b.d.l.	b.d.l.	100
	S62	61,29	12,5	b.d.l.	0,52	10,73	b.d.l.	14,97	b.d.l.	b.d.l.	100
	S63	61,17	11,64	b.d.l.	0,39	10,49	b.d.l.	13,4	1,68	1,24	100
DDH-04-44.5m	a	62,33	12,26	0,73	0,61	6,63	2,93	14,5	b.d.l.	b.d.l.	100
	b	61,33	12,78	0,99	b.d.l.	6,87	2,99	15,03	b.d.l.	b.d.l.	100
	c	61,87	12,75	1	b.d.l.	9,42	b.d.l.	14,96	b.d.l.	b.d.l.	100
	d	60,94	13,01	0,6	b.d.l.	5,75	4,65	15,05	b.d.l.	b.d.l.	100

Tabla 4 - Semi-quantitative chemical analyzes in plumbojarosite

	Element	O	Na	Al	Si	S	K	Ca	Fe	Cu	Zn	Ga	As	Ag	Cd	In	Pb	Total:
	Analysis	Wt%																
DDH-04; 7469	S79	60.39	b.d.l.	0.37	0.31	07.01	1.69	b.d.l.	19.64	b.d.l.	b.d.l.	b.d.l.	0.96	b.d.l.	b.d.l.	0.39	9.24	100
	S80	59.39	1.16	0.21	0.13	8.18	1.85	b.d.l.	16.71	b.d.l.	b.d.l.	b.d.l.	1.12	b.d.l.	b.d.l.	0.21	11.05	100
	S81	64.27	1.56	0.19	dld	7.67	1.62	b.d.l.	14.52	b.d.l.	b.d.l.	b.d.l.	01.05	b.d.l.	b.d.l.	0.31	8.8	100
	S83	59.31	0.97	0.48	0.34	5.66	1.28	b.d.l.	21.22	b.d.l.	b.d.l.	b.d.l.	01.03	b.d.l.	b.d.l.	0.31	9.4	100
	S99	58.87	2.48	0.44	0.86	6.99	2.2	0.76	17.6	b.d.l.	b.d.l.	b.d.l.	0.85	b.d.l.	b.d.l.	0.12	8.83	100
	S100	61.13	1.65	0.27	b.d.l.	8.43	02.09	b.d.l.	19.6	0.15	0.02	b.d.l.	0.68	0.06	0.12	0.01	5.8	100
	S101	59.62	1.78	0.24	0.21	8.22	1.64	b.d.l.	21.38	b.d.l.	b.d.l.	b.d.l.	0.84	b.d.l.	b.d.l.	0.12	5.95	100
	S102	58.39	b.d.l.	0.35	0.33	5.78	1.34	b.d.l.	23.13	b.d.l.	b.d.l.	0.07	1.18	b.d.l.	b.d.l.	0.44	9	100

	Element	O	Na	Al	Si	S	K	Ca	Fe	Cu	Zn	Ga	As	Ag	Cd	In	Pb	Total:
	Analysis	Atomic %																
DDH-04; 7469	S79	84,38	b.d.l.	0,31	0,24	4,89	0,97	b.d.l.	7,86	b.d.l.	b.d.l.	b.d.l.	0,29	b.d.l.	b.d.l.	0,08	1	100
	S80	83,48	1,13	0,17	0,1	5,74	1,07	b.d.l.	6,73	b.d.l.	b.d.l.	b.d.l.	0,34	b.d.l.	b.d.l.	0,04	1,2	100
	S81	85,61	1,45	0,15	dld	5,1	0,88	b.d.l.	5,54	b.d.l.	b.d.l.	b.d.l.	0,3	b.d.l.	b.d.l.	0,06	0,9	100
	S83	83,68	0,95	0,4	0,27	3,98	0,74	b.d.l.	8,58	b.d.l.	b.d.l.	b.d.l.	0,31	b.d.l.	b.d.l.	0,06	1,02	100
	S99	81,81	2,4	0,36	0,68	4,85	1,25	0,42	7	b.d.l.	b.d.l.	b.d.l.	0,25	b.d.l.	b.d.l.	0,02	0,95	100
	S100	82,85	1,56	0,22	b.d.l.	5,7	1,16	b.d.l.	7,61	0,05	0,01	b.d.l.	0,2	0,01	0,02	b.d.l.	0,61	100
	S101	82,03	1,71	0,2	0,17	5,64	0,92	b.d.l.	8,43	b.d.l.	b.d.l.	b.d.l.	0,25	b.d.l.	b.d.l.	0,02	0,63	100
	S102	83,57	b.d.l.	0,3	0,27	4,13	0,79	b.d.l.	9,48	b.d.l.	b.d.l.	0,02	0,36	b.d.l.	b.d.l.	0,09	0,99	100